

Energy, ropelength, and other physical aspects of equilateral knots

Kenneth C. Millett

*Department of Mathematics
University of California, Santa Barbara
Santa Barbara, CA 93016 USA
Email: millett@math.ucsb.edu*

Eric J. Rawdon

*Department of Mathematics and Computing
Chatham College
Pittsburgh, PA 15232 USA
<http://monkey.chatham.edu/~rawdon>
Email: rawdon@chatham.edu*

Abstract

Equilateral spatial polygons provide useful models of spatial knots and the spaces of such knots. Associated to these configurations are energies, ropelength or thickness, crossing number, writhe, and other measures reflecting the spatial structure such as the volume and surface area on the convex hull. The optimization of the energy and the ropelength and physical and spatial characteristics of optimized configurations are the subject of this paper. Data from computer explorations of these facets of physical knot theory is presented and discussed.

Key words: Equilateral Knots, Polygonal Knots, Knot Space, Thickness, Ropelength, Knot Energy

1 Introduction

The goal of this research is the exploration of spatial parameters, including “energy” and “ropelength”, by which polygonal and equilateral knots are evaluated in the search for optimal conformations or which provide information about the spatial aspects of their situations. The optimal conformations are geometrically equivalent polygons in which the relevant quantity has achieved an extreme or optimum value. Such conformations are commonly proposed as

models for the most likely or average positions observed for macromolecules arising in physics and molecular biology [1–4]. Their properties are thought to be related to critical physical characteristics arising from simulations and from experiments, e.g. time-averaged shapes of DNA molecules in solution, the speed of migration in gel electrophoresis of DNA knots, and sedimentation coefficients of DNA. We will also consider properties of the knot spaces and their relationship with several of the quantitative descriptors associated with the optimal configurations. We will look at how they are related to the specific knot type as well as the specific optimizing quantity.

By a *polygonal knot* we will mean the spatial polygon determined by a specified finite number of points in three-space that are connected to each other in a given cyclical fashion. Such knots, with the additional specification of a distinguished vertex and an orientation, are naturally identified with points in a subset of the Euclidean space of dimension three times the number of points. It is a proper subset since singularities such as self-intersections of edges are not allowed. If the lengths of the segments connecting the successive vertices of the polygon have unit length, the result is an *equilateral knot*. Such knots are constrained to a subspace of dimension twice the number of vertices. Two conformations are equivalent if one can move from one to the other by a path within the respective “knot space.” The structure of these knot spaces allows one to ask for the proportion of the space consisting of knots of a specific topological type. That is, “For a given specific number of randomly selected vertices, what is the probability the knot they determine is of a specific topological type?” For a fixed number of vertices, this imposes a natural order on the topological knot types determined by decreasing probability of occurrence.

Following a technical introduction to the fundamental concepts with which we will be concerned, we will discuss the topology of the associated knot spaces. We will then present the results of computer experiments seeking the optimization of both energy and ropelength of equilateral polygonal knots as well as the calculation of such secondary quantities for these “optimal” configurations as the average crossing number and average writhe. These secondary quantities are those thought to connect the natural instances of the knot conformations to observed behavior.

We will also explore the degree to which optimal conformations are spatially similar. In simulations of optimization procedures, one can arrive at apparent local optima whose graphical representations look very different. To what extent are these visual differences reflective of truly distinct conformations and to what extent are the seeming differences merely manifestations of different perspectives on the same or similar conformations? The choice of knot thickness shown in the figures was determined by the desire to provide a clear illustration of the phenomena in question. These are not, in general, the thickness of the configuration. We will consider several fundamental ways in which

to associate characteristic quantities to the conformation that will facilitate comparison and which promise to quantify the degree to which these conformations are different. One example is the dimensions of the smallest rectangular box containing the conformation. Others include the surface area and volume of the convex hull of the knot.

All of these quantities lie within the domain of physical knot theory. From this perspective, the goal is the determination of “natural” quantitative spatial characteristics that provide a quantitative linear order of knotting that strongly correlates with the observed physical behaviors, in terms of both order and relative magnitude of the observed quantities. Using the physical knot characteristics considered in this paper we compare the degree to which they are consistent with experimental observations from the study of DNA.

2 Knot Spaces

In this section we will briefly review some of the basic definitions and concepts so as to give a concrete foundation to our later discussion. Fuller treatments of this topic can be found in papers of Calvo, Millett, and Randell [5–11]. By a geometric or polygonal knot we mean an embedding in Euclidean three-dimensional space of an oriented regular polygon which is linear on its edges. *Singular knots* are those maps which do not give embeddings of the polygon. The polygon has a specified number of vertices, one of which has been selected to serve as a starting point or first vertex of the polygon. The identification of a second vertex is equivalent to the determination of an orientation of the polygon. Each such embedding is determined uniquely by the image of the associated vertices, starting at the first and proceeding in the direction determined by the orientation. This choice of initial vertex and orientation, therefore, allows one to uniquely associate to each embedding a point in a Euclidean space of dimension equal to three times the number of vertices. By fixing the number of vertices, n , we determine an open subset of this Euclidean space, $Geo(n)$, corresponding to these embeddings. The complement is a closed set of codimension one corresponding to maps with self-intersections or other failures of the embedding property. If we require the embeddings to be length-preserving, we define the subset of equilateral knots, $Equ(n)$. This latter knot space is a manifold of dimension equal to twice the number of vertices. The path components of $Geo(n)$ or $Equ(n)$, i.e. the sets of those knots that can be connected to each other by paths or deformations within the respective knot space, define the geometric or equilateral knot types. Thus, if two geometric knots lie in the same component, we say that they are geometrically equivalent. Similarly, two equilateral knots are equilaterally equivalent if they lie within the same component of $Equ(n)$. Note that, in the case of equilateral knots, we do not allow the length of the edges to change. While allowing the length

of edges to change, while still preserving the equality of the lengths, gives an equivalent theory on knotting, we have chosen to require the edge lengths to be fixed as seems more appropriate in terms of applications to the natural sciences. Recall that a classical theorem of Whitney [12] guarantees that there are only finitely many geometric or equilateral knot types for each n .

In general, these knot types are finer than the topological knot type, even when one has removed the specification of orientation and base vertex. Calvo [5,6] has shown that the first example of this phenomena occurs with the heptagonal figure-8 knots. Topologically, the figure-8 knot is equivalent to its mirror reflection but, for heptagons, there are two distinct classes of figure-8 knots interchanged by mirror reflection. Although, in this project, we are principally concerned with the topological type of the knot, we will restrict ourselves to deformations within the various geometric knot types when considering questions of optimization of spatial knot parameters. Therefore, it is important to realize that there may be more than one equilateral knot type corresponding to a given topological knot type. Consequently, it is possible that there are fundamentally different optimal geometric realizations of a topological knot type.

This is a potentially serious problem deriving from the difference between topological knotting and geometric knotting. In the cases discovered by Calvo, [5,6], the action of the dihedral group implies that optimal configurations are equivalent. But, in general, we do not have such knowledge and it may well be the case that different geometric knot components will have fundamentally distinct optimal configurations for a specific optimizing quantity. As changes in orientation or base point can be accomplished by isometries of the knot space, i.e. homeomorphisms or equivalences preserving the distance structure, this restriction to based oriented configurations does not result in any loss of generality. In addition, there are locally optimal configurations having quite different parameters and spatial characteristics. As a consequence, proposed optimal configurations are, in fact, conjectures due to the absence of sharp estimates of the optimal parameter values.

For a fixed number of vertices, all planar embeddings of polygons determine equivalent knots, equivalent to the standard regular polygon. This class is called the unknot or the trivial knot, independent of the number of vertices. The first case of a non-trivial knot occurs with six edges. In $Geo(6)$ and $Equ(6)$, Calvo has shown that there are precisely five components or knot types. Topologically, these correspond to one component of unknots and two each of left-handed and right-handed trefoils, one of which is shown in Figure 1. In $Geo(7)$ and $Equ(7)$ a new topological knot type occurs, the Listing or figure-8 knot.

Calvo shows that there are exactly five components in $Geo(7)$, one each of

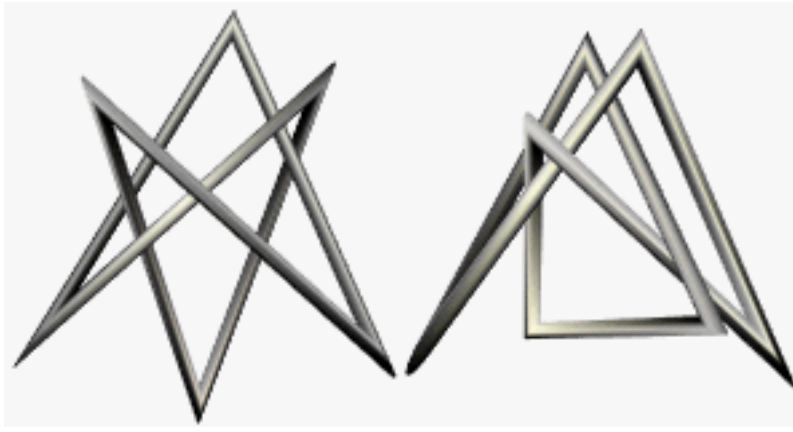


Fig. 1. A hexagonal trefoil knot and a heptagonal figure-8 knot

unknots, right-handed and left-handed trefoils, and two components of figure-8 knots, an example of which is shown in Figure 1. These components are preserved under mirror reflection, i.e. the geometric knots are achiral, but are not preserved under change of orientation, i.e. the heptagonal figure-8 knot is not reversible. Since the topological figure-8 knot is reversible, this identifies one difference between geometric knot theory and classical topological, piecewise linear, or smooth knot theory. For $Geo(8)$, Calvo and Millett have shown [13] that the only topological knot types that occur are, using the classical notation, 0.1, 3.1, 4.1, 5.1, 5.2, 6.1, 6.2, 6.3, 8.19, 8.20, $3.1\#3.1$, and $3.1\#-3.1$. The latter knots are the connect sums of the trefoil with itself (the “granny” knot) and with its mirror reflection (the “square” knot).

Using Metropolis Monte Carlo methods, Millett [8,13,14], has provided estimates of the topological types of geometric and equilateral knots for larger numbers of edges by calculation of the HOMFLY polynomials that are observed. These computational experiments have provided examples of nine edge knots for which the polygonal number of a topological knot type, i.e. the minimal number of edges required to construct a geometric knot of a given topological knot type, is thereby determined.

In this paper we will focus on the equilateral knot spaces for 8, 16, and 32 edges. There are 12 topological types for the polygonal octagonal knots, up to mirror image, giving 20 distinct HOMFLY polynomials. While only 12 of the 20 polynomials have been observed in the Monte Carlo study of equilateral octagonal knots, all but one of the topological knot types has been constructed as an equilateral knot. The exception, at the time of this paper, is 8.19. We have not been able to construct an octagonal equilateral representative of this topological knot type nor have we been able to show that such an example is impossible. Thus there are eight polynomials of equilateral octagonal knots that have not yet been observed, of which seven are known to represent actual configurations. For 16 edge equilateral knots, some 106 distinct HOMFLY

polynomials have been observed, and for 32 edge edge equilateral knots, 484 distinct polynomials have been observed. In contrast, for geometric knots, 201,736, and 327,433 distinct HOMFLY polynomials have been observed, respectively. While the estimated rate of growth of equilateral knots is less than that of geometric knots, both populations have an exponential growth. In a carefully studied 50 edge equilateral knot experiment, 2,952 distinct HOMFLY polynomials were observed of the predicted total of 3,472 distinct HOMFLY polynomials [13].

The population base for the computational study of equilateral knots, whose results are reported in this paper, is those 102 topological knot types, prime and composite, through 9 crossings. While, as noted above, only 11 of these have been constructed with 8 edges, all of these knots can be constructed with 16 edges. The 32 edge knots in this study are constructed by subdividing the 16 edge knots. In the 16 edge Monte Carlo exploration, we observed topological knot types with more than 9 crossings, but did not observe all of the 9 crossing knots that we were able to construct explicitly. Deformations are allowed to occur in the respective knot spaces even though the initial embeddings arose with fewer edges.

The topology and the geometry of knot space plays a critical role in understanding the conceptual basis of this research. In the case of $Geo(n)$ and $Equ(n)$, we will use the structure induced from the Euclidean spaces in which they naturally lie. Thus, $Geo(n)$ is a $3n$ -dimensional open submanifold of $3n$ -dimensional Euclidean space and $Equ(n)$ is the codimension n quadric subvariety of $Geo(n)$ defined by the requirement that all edges have unit length. Since the point $(1, 1, \dots, 1)$ is a regular value of the function, $f : Geo(n) \rightarrow \mathbb{R}^n$ that calculates the length of the individual edges (Corollary 1, [11]), $Equ(n)$ is a smooth $2n$ -dimensional submanifold of $Geo(n)$.

It is convenient to consider the subspaces defined by requiring that the first vertex be at $\{0, 0, 0\}$, i.e. we factor out the Euclidean translations. These spaces are denoted $Geo_0(n)$ and $Equ_0(n)$, respectively. The geometric knot types, i.e. the connected components, in $Geo(n)$ and $Geo_0(n)$ are invariant under homotheties of 3-space. This shows that the structure of these spaces can be studied by considering their intersection with the unit sphere or unit ball in $3n$ -space. $Equ(n)$ and $Equ_0(n)$ are subsets of the smooth sphere of knots whose total edge length is equal to one (of course some edges may be degenerate) and, therefore, have compact closure in this sphere. These compactifications allow us to estimate the fraction of the space consisting of knots of a specified topological knot type or, equivalently, the probability that a randomly selected geometric knot will be of specific topological knot type.

The fact that $Equ(n)$ and $Equ_0(n)$ are submanifolds of Euclidean space will play a significant role in the application of numerical methods to their com-

puter assisted exploration. A knot K is determined by its vertex set, $K = \{v_0, \dots, v_{n-1}\}$. We denote the edges of K by $e(K) = \{e_0, \dots, e_{n-1}\}$ with e_i denoting the edge connecting v_i to v_{i+1} and e_{n-1} connecting v_{n-1} to v_0 . Let δ denote the standard metric on \mathbb{R}^3 . Extend this metric to \mathbb{R}^{3n} by taking the maximum of its values on each of the n three-dimensional subspaces, that is

$$\delta(\{v_0, \dots, v_{n-1}\}, \{w_0, \dots, w_{n-1}\}) = \max_{0 \leq i \leq n-1} \delta(v_i, w_i).$$

The induced metric on $Equ(n)$ and $Equ_0(n)$ is denoted by $\delta(K, K')$ where $K = \{v_0, \dots, v_{n-1}\}$ and $K' = \{w_0, \dots, w_{n-1}\}$. This metric will play an important role in the study of the structure of knot spaces.

Definition 1 *For a knot, K , in $Geo(n)$, define $\mu(K)$ to be the minimum of the minimum distances between non-adjacent edges of K .*

We note that $\mu(K)$ is no larger than the length of the shortest edge of K .

Definition 2 *Let $Tube(K, r)$ to be the union of open balls centered at the vertices of K and of open cylindrical tubes with the edges of K as axes, both of radius r .*

Proposition 3 *For any $r < \frac{\mu(K)}{2}$, $Tube(K, r)$ is an embedded torus whose center curve is K .*

PROOF. The balls of radius r centered at the vertices are pairwise disjoint as each vertex belongs to a non-adjacent edge. The union of the cylinders associated to an edge and the ball associated to the vertices of the edge is a convex region that is, therefore, topologically a ball. Two such balls intersect only if they are associated to adjacent edges. In this case, their intersection is a convex ball containing the ball of radius $\frac{\mu(K)}{2}$ centered at their common vertex. The proposition is proved by taking the union of these balls following an increasing arc of edges in K . By induction, until the last edge is reached, at each stage one has the union of a ball, with a convex ball associated with the next edge. The intersection is a convex ball. The result is, therefore, a ball. In the case of adding the final edge, the intersection consists of two disjoint convex balls. The resulting union is the required torus. \square

Corollary 4 *Every knot, K' , with $\delta(K, K') < \frac{\mu(K)}{2}$ lies within $Tube(K, \frac{\mu(K)}{2})$ and is geometrically equivalent to K by a path of geometric knots lying within the tube.*

PROOF. This isotopy is defined by moving the vertices of K' to those of K radially within the ball neighborhoods of the vertices of K and extending linearly to the associated edges. \square

One way in which to interpret this result is to say that all knots, K' , within the ball centered at K of edge length $\frac{\mu(K)}{2}$ are non-singular and geometrically equivalent to K . That is to say that the map from the regular polygon to the vertices of K' is an embedding and that there is a path connecting K' to K consisting of such knots. Note that the “ball” in this metric is actually the product of n 3-dimensional balls. As such, it might better be imagined as a “cube” centered at K of edge length twice the radius of the ball. The open ball centered at K with radius $\frac{\mu(K)}{2}$ is the largest ball centered at K that does not intersect the singular set, i.e. lying entirely within the component of knots containing K , since any larger radius would permit the intersection of non-adjacent edges. If the edge lengths are relatively small compared to the separation of distant edges, the first singularities that arise with expanding radius correspond to “type I Reidemeister” singularities that do not create different geometric knot types.

The radius of the ball neighborhood of K disjoint from other geometric knots types is related to the radius of the tubular neighborhood of K . It is a measure of the “thickness” of K , a spatial or physical aspect of the knot reflecting the degree to which perturbations of K do not change the knot type. Another physical way to understand the role of K is as an “average” of the knots in the ball of which it is the center. The study of such physical characteristics of polygonal knots is a principal objective of this paper and it is the subject of the next section.

3 Physical Knot Theory

We use the term “physical knot theory” to refer to those aspects of knots that arise in the study of physical models and which are captured by the geometry of the polygonal knot configuration. Our first example is that of a knot energy. This notion is inspired by the desire to create a dynamical method to realize a family of allowable transformations taking any given manifestation of a topological unknot to the standard unknot. Minimal energy conformations have been proposed as “canonical models” of the knot type and these energies are cited as examples of knot invariants. An initial proposal for an energy consisted of a uniform charge along the knot which was subjected to an inverse-square repulsion force. There are many examples of energies that have been proposed, each with different properties [15–32]. While much has been learned, the original goal of this project has yet to be accomplished. In this paper we shall employ a version of the O’Hara [24] and Freedman-He-Wang Möbius energy [19], that has been adapted to polygonal knots from their formulation for smooth knots. This adaption is, in fact, an energy proposed and studied by Jon Simon [28]. Simon defines an energy to be the sum, over non-adjacent edges of the polygon, of the product of the lengths of the edges divided by

the square of the minimum distance between the edges. By subtracting an intrinsic term, the energy of the regular n -gon, one defines a regularized energy, $E_{MD}(K)$, that approximates half the value of the integral giving one form of the Möbius energy. In this normalization, the regular n -gon has energy 0. By giving an explicit estimation of the error, Rawdon and Simon [33] have demonstrated the convergence of $E_{MD}(K)$ to half of the Möbius energy as the number of edges increases and the polygonal knot “approaches” a smooth conformation.

A second example of a physical knot property is the thickness and ropelength of the polygonal knot configuration. The injectivity radius, $R(K)$, of a smooth knot conformation, K , is the supremum of the radii such that normal discs of that radius at each point of the knot are disjoint. By dividing the injectivity radius by the arc length of the knot, we obtain a scale-invariant quantity called the thickness, $\tau(K)$, of the knot that measures how thick this knot could be when tied with a unit length cord. The reciprocal of $\tau(K)$ is called the ropelength, $\rho(K)$, of the knot [32]. This measures the shortest length of unit radius cord needed to tie the knot. The injectivity radius is shown to be the minimum of $MinRad(K)$ and $\frac{1}{2}DSCD(K)$ where $MinRad(K)$ is the minimum of the radius of curvature of K and $DSCD(K)$ (doubly-critical self-distance) is the minimum distance between pairs of distinct points whose connecting segment is perpendicular to the tangents to the knot at both points.

Rawdon [29–31] has provided an analogous definition of injectivity radius for polygonal knots and, as above, provides definitions of thickness and ropelength. The polygonal thickness and ropelength functions have the property of convergence to the corresponding quantities for smooth knots, for families of inscribed polygons converging to the smooth knot. Rawdon’s polygonal injectivity radius is the minimum of a polygonal version of the doubly-critical self-distance function and a minimal radial distance arising from the adjacent edges due to curvature.

A third example is the average crossing number of the configuration. Here, one takes the average of the number of crossings, over all generic planar projections of the configuration. By assigning a sign, +1 or -1, to each of these finitely many crossings and taking the algebraic sum averaged over all generic projections, one defines the average writhe of the configuration. Average writhe is often referred to as just writhe. However, we use the term average writhe to highlight its relationship with the average crossing number and to stress that the quantity is measured on a conformation, not a knot type. There is a wide variety of quantities that can be defined by this averaging procedure, several of which have provided important information about knots in the past. Another example is given by the average number of maxima of projections to lines in three space over all possible line directions. This average is equal to the total curvature of the configuration, i.e. the sum of the exterior angles at

each of the vertices [34,35].

The large scale “shape of a configuration” is another facet of physical knot theory. In this paper we will focus on the comparison of the shape of two knots having the same number of vertices in an optimal configuration with respect to ropelength or energy. Two knots would have the same “shape” if they are sufficiently close in knot space or, more generally, if there is an isometry of knot space taking one sufficiently near the other. Thus our measures of shape should be continuous functions of the knot, as determined by the vertices, and should be invariant under isometries of knot space. Among such physical shape properties of a knot are the volume, surface area, and dimensions of a smallest standard shape containing the knot. One step in this direction is the shape of a standard smallest rectangular box containing the knot. The dimensions of the box give a rough quantitative description of the spatial shape of the knot. Is the knot “squat and broad,” “bulbous,” or “long and skinny?” These dimensions can provide a crude indication of such spatial characterizations. We will call the largest dimension, the box length of the knot. The standard box for a given polygonal knot, K , is defined as follows: the length of the polygonal knot, K , is defined to be the maximum distance between the vertices, $BL(K)$. Consider the projection of K to a plane perpendicular to the line passing through these extremal vertices (or the set of such projections, if there are more than one pair) and take the pair of image vertices of maximal distance. Define this distance to be the width of K , $BW(K)$. Finally, in this plane, project the image of K to a line perpendicular to the line passing through these extremal vertices (or the set of such projections, if there are more than one pair) and take the pair of image vertices of maximal distance. Define this distance to be the height of the knot, $BH(K)$. The vertices defining the box length, box width, and box height of K determine a box containing K as well as the shape of this box.

Proposition 5 *Let a non-trivial knot, K , have maximal thickness (i.e. minimal ropelength) in its equilateral knot type. The box length of the knot is $\geq \mu(K)$. The box height of knot K is $\geq \mu(K)$.*

PROOF. The quadrisecant theorem, [36–39], states “Every non-trivial piecewise linear or smooth knot in general position has four collinear points.” The separation between any pair of the four points must be at least equal to $\mu(K)$ if they involve non adjacent edges. At least two of these of these points are not adjacent on the knot. Their distance is at least $\mu(K)$ giving this as a strict lower bound for the box length. The projection of K to the plane perpendicular to the height direction is close to a regular projection. $\mu(K)$ is the minimum distance between non adjacent edges. Crossings, therefore, have a difference in height at least $\mu(K)$. This height difference is no larger than the box height of the knot. \square

In fact, one expects that three $\mu(K)$ is the lower bound of the box length. This is the case for minimal edge equilateral knots of maximal thickness because the triangle determined by any pair of adjacent edges must be pierced by a distant edge, i.e. one whose distance from each of the adjacent edges is at least $\mu(K)$. For equilateral knots with a large number of edges, compared to the edge number, the collinear points are non adjacent. In this case $\mu(K)$ is not controlled by the edge length and the quantity of interest is the thickness of the knot.

Other interesting physical properties of the knot are the volume and surface area of the associated box. They reflect the “density of the knot” and the “accessibility of the knot.” The smaller the volume of the box, the more tightly or more densely packed the knot. Similarly, the larger the surface area of the box, the more exposed the knot will be to contact from the exterior. We will also consider a related approach to assessing the density and accessibility of a knot by means of the surface area and volume of the convex hull of the knot.

For knots having a spherical or cubical shape, the volume is proportional to the $3/2$'s power of the surface area. If, on the other hand, the knot has a broad squat cylindrical shape, the volume will be approximately a linear function of the surface area. Thus one useful measure of the shape of a knot, its density and accessibility, is the functional relationship between volume and surface area. The surface area/volume relationship should also be dependent on the number of vertices in the optimal configuration and the polygon number of the knot. For example, when the number of vertices is close to the polygon number, the knot is “difficult to construct” and is quite likely to be flatter and broader in nature compared to optimal configurations of the same knot type with more vertices. There are an insufficient number of edges to achieve a truly thick conformation. While this appears to often be the case, by analysis of individual knot types, one will see that the data shows a far more complex relationship between the number of edges and the spatial shape of the conformation associated to a given topological knot type as the number of edges increases.

We will also explore the potential for an elementary relationship between these physical aspects of an optimal exemplar of an equilateral knot type and the size of the component of equilateral knots having the same topological knot type. For example, one might expect that knots whose optimal conformations are quite thick or whose convex hulls have larger volume would be more likely to occur than those that are thinner or whose convex hulls have small volume or which are relatively squat. Thus, we explore the degree of correlation between these physical quantities and the relative probability of the geometric knot type.

4 Estimation of Physical Knot Properties

In this study of physical knot properties we employ Metropolis Monte Carlo [40] population estimations, weighted random walk optimizations, and other computer-based calculations involving knots in $Equ(n)$. The very nature of such numerical calculations, however, takes one out of $Equ(n)$ into $Geo(n)$ by virtue of the fact that calculations are not exact. The purpose of this section is to discuss our methods and to explain why the calculations, although not exact, do provide estimates of quantities actually associated to $Equ(n)$.

One underlying principle is the existence of a tubular neighborhood of $Equ(n)$ in $Geo(n)$. This structure provides a retraction of a neighborhood of $Equ(n)$ that respects the geometric knot type. In other words, if there is an approximately equilateral knot, then there is a geometrically equivalent equilateral knot nearby. The definition of “approximately equilateral knot” includes a specific estimate of how close to length one the edges must be in order to apply the theorem. The result is a condition that is easily verified during the calculation in computer simulations and implies the existence of an equilateral knot with the desired properties. A second consequence is a condition on how close a deformation in $Geo(n)$ of an equilateral knot must remain to $Equ(n)$ in order to insure that a purely equilateral deformation exists.

These results derive from a study of the regular values of the function, $L : Geo(n) \rightarrow \mathbb{R}^n$, that calculates the lengths of the edges. Thus, while the optimization algorithms in theory take elements of $Equ(n)$ to elements of $Equ(n)$ through various geometric movements, the numerical nature of the computer implementation of the algorithm actually takes one out of $Equ(n)$ into $Geo(n)$. The accuracy of the algorithms insure that the result remains near $Equ(n)$ in a measurable way that insures that nearby elements or paths in $Equ(n)$ exist. These quantities are continuous functions on $Geo(n)$ so, as a consequence, the calculated values are close to those of the element of $Equ(n)$ whose existence has been demonstrated.

Another way in which the calculations are often estimates rather than precise calculations derives for the fact that the HOMFLY polynomial, [41,42] is used as a surrogate for the topological knot type. This is not a faithful representation [43]. Furthermore, we do not identify chiral representatives as is often customary in knot theory nor is the HOMFLY polynomial successful in always distinguishing chiral knots. As a consequence our estimates of knot types are estimates of the chiral knot types, and limited by the lack of faithfulness of the HOMFLY polynomial as well as the fact that they are statistical estimates derived from our simulations.

Proposition 6 *If a geometric knot is sufficiently close to being equilateral,*

there is a nearby equilateral knot of the same geometric knot type.

PROOF. Suppose that K is a geometric knot whose edge lengths are within ϵ of being unit length, i.e. if L_i denotes the length of the i th edge, then $|L_i - 1| < \epsilon$. We first describe the construction of an equilateral knot, K' , near K . Suppose that the vertices of K and K' are denoted by v_i and v'_i respectively. Let $v'_0 = v_0$ and define v'_1 by $v'_0 + \frac{v_1 - v'_0}{\|v_1 - v'_0\|}$ so that the first edge has unit length. The key issue is the distance between v_1 and v'_1 since this will determine the degree of edge length distortion of the geometric knot.

$$\begin{aligned}\|v_1 - v'_1\| &= \left\| v_1 - \left(v'_0 + \frac{v_1 - v'_0}{\|v_1 - v'_0\|} \right) \right\| \\ &= \left| \|v_1 - v'_0\| - 1 \right| \\ &= |L_0 - 1| \\ &< \epsilon.\end{aligned}$$

For $1 < i < n - 1$, we define $v'_i = v'_{i-1} + \frac{v_i - v'_{i-1}}{\|v_i - v'_{i-1}\|}$ and compute that

$$\begin{aligned}\|v_i - v'_i\| &= \left\| v_i - \left(v'_{i-1} + \frac{v_i - v'_{i-1}}{\|v_i - v'_{i-1}\|} \right) \right\| \\ &= \left| \|v_i - v'_{i-1}\| - 1 \right| \\ &< i\epsilon.\end{aligned}$$

This follows, by induction, from the fact that

$$\begin{aligned}1 - \epsilon - (i - 1)\epsilon &< \|v_i - v_{i-1}\| - \|v_{i-1} - v'_{i-1}\| \\ &\leq \|v_i - v'_{i-1}\| \\ &\leq \|v_i - v_{i-1}\| + \|v_{i-1} - v'_{i-1}\| \\ &< 1 + \epsilon + (i - 1)\epsilon.\end{aligned}$$

In order to insure that the last two edges have unit length, a slightly more careful choice of v'_{n-1} is required. Note that the v_{n-2} , v_{n-1} , and v_0 determine an almost isosceles triangle with almost unit length legs having the v_0 and v_{n-2} as end points of its base. Except in degenerate situations, the new vertex, v'_{n-1} , can be selected to lie in the plane determined by this triangle such that the isosceles triangle it determines, with the edge connecting v_0 and v'_{n-2} as its base, will have exactly unit length legs. Degenerate cases occur when the three vertices are collinear or when the distance between the v_0 and v'_{n-2} is

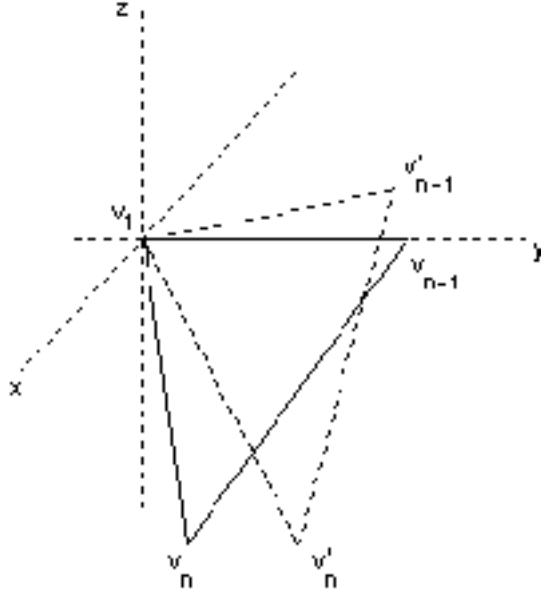


Fig. 2. Selecting v'_{n-2} and v'_{n-1}

either 0 or is 2 or larger, otherwise the choice is a continuous function of the coordinates of v'_{n-2} and converges to the isosceles vertex associated to v_0 and v_{n-2} as v'_{n-2} tends toward v_{n-2} . Then v'_{n-1} is close to v_{n-1} .

These facts can be verified analytically by considering, without loss of generality, the case in which the first vertex is at the origin, the $(n-2)$ nd vertex is a point $\{0, y, 0\}$ and, $n-1$ st vertex is in the first quadrant of the xy -plane, close to the point $\left\{\sqrt{1-\frac{y^2}{2}}, \frac{y}{2}, 0\right\}$. The new $(n-2)$ st vertex is at the point $\{r, y+s, t\}$ with the magnitude of the vector $\{r, s, t\}$ less than $(n-1)\epsilon$.

The selection of the $(n-2)$ st vertex is a smooth function of its variables except possibly at $y=0$ or $y \geq 2$. The case $y=0$ represents a singular position that can be avoided by selecting v'_{n-2} to be on the unit sphere centered at v'_{n-2} close, but not equal, to the singular position determined by the formula. The situation for $y \geq 2$, represents another singular position and care must be exercised to insure that an impossible configuration is not imposed by the choice v'_{n-2} . In this case, the distance between v_0 and v_{n-2} is less than $2+2\epsilon$. The vertex v'_{n-2} can be chosen to be on the interval connecting these vertices at distance 2 from v_0 and v'_{n-1} can be chosen to be the midpoint of the interval connecting v_0 and v'_{n-2} . In this case, v'_{n-2} is within 2ϵ of v_{n-2} and v'_{n-1} is within $2\sqrt{\epsilon}$. \square

Corollary 7 *Every n edge almost equilateral knot, K' , with*

$$|L_i - 1| < \min\{\mu(K)/n, \mu(K)^2/4\}$$

where L_i denotes the length of the i th edge, is equivalent to an equilateral knot K .

For example, the seven edge “almost equilateral” figure-eight knot shown in Figure 1 has $\mu \approx 0.027727$ while the maximal difference of the edge length from 1 is less than 0.000001 proving the existence of an equilateral figure-eight knot.

Theorem 8 *For each equilateral knot, K , there is an $\epsilon(K) > 0$, such that any equilateral knot, K' , within $\epsilon(K)$ of K is equivalent to K by a sequence of pivots, translations, and rotations.*

PROOF. Starting at the distinguished vertices, move the first vertex of the first knot to the first vertex of the second via a translation. By a rotation, move the second vertex of the first knot to the second vertex of the second knot. We proceed by induction on the vertices which differ. Suppose the positions of the vertices, v_j and v'_j respectively, of the two knots are identical through the first j vertices.

Suppose $j < n - 2$. In the plane determined by the vertices v_{j+1} , v_{j+2} , and v_{j+3} of the first knot, there is a new vertex, v''_{j+2} , such that, in the vertex set of the first knot, the result of replacing the v_{j+2} with v''_{j+2} and replacing v_{j+1} with v'_{j+1} , is a new equilateral knot near the second knot and with vertex agreement through the first $(j + 1)$ vertices. K and this new knot are connected by a sequence of three small rotations, see Figure 5, as follows. By a small rotation about the axis determined by the vertices v_{j+1} and v_{j+3} of the first knot, move the v_{j+2} such that its distance from v_j and the distance of v''_{j+2} from v_j are equal. Next, by small rotation about the axis determined by the v_j and v_{j+3} , move v_{j+1} and v_{j+2} until the later coincides with v''_{j+2} . The third, and final rotation in this sequence, is about the axis determined by v''_{j+2} and v_j . This small rotation takes v_{j+1} of the first knot to v'_{j+1} .

If $j = n - 2$, take the rotation using the v_{n-2} and the v_0 as the axis to achieve the final coincidence of the last vertices. \square

Corollary 9 *If two equilateral knots are of the same geometric knot type by virtue of a path of geometric knots that are sufficiently close to being equilateral at each stage, there is an equilateral equivalence of the two knots.*

PROOF. Using the compactness of the path, one approximates by small intervals, the path by almost equilateral knots with a sequence of equilateral knots that are sufficiently close so as to be connected by a sequence of pivots, translations, and rotations as provided by Theorem 8. \square

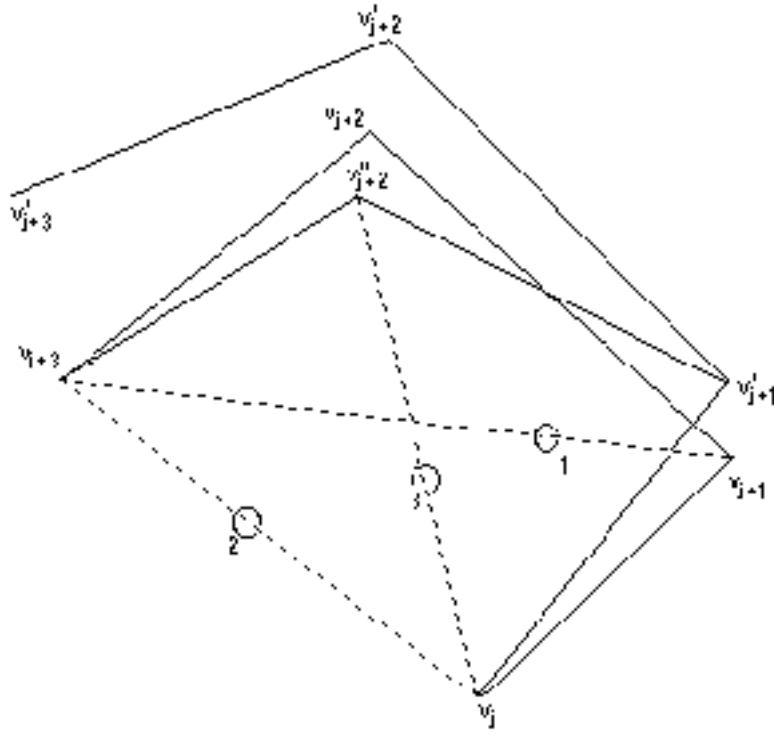


Fig. 3. The three step move

Corollary 10 *Any path in $Equ_0(n)$ can be approximated arbitrarily closely by a path consisting of pivots, rotations, and translations.*

Theorem 8 has important implications with respect to computer optimization of energy and ropelength for knots in $Equ(n)$. The optimization strategy employed, with various modifications, has the following structure. First, with respect to uniform distributions, two knot vertices and a rotation angle are selected within the relevant tolerance range necessary to preserve the knot type. A test conformation is constructed by means of a pivot of the chosen angle about the axis specified by the two vertices applied to the vertices lying along one of the arcs between the selected vertices. The quantity to be optimized is calculated for the test conformation and the value compared to the current value. If better, the test case replaces the current case and the procedure continues. In some of our algorithms, the successful pivot data is used again, perhaps with modification, until no further improvement is observed. If there is no improvement, a new choice of angle and vertices is tested. Since spatial rotations and translations are isometries of 3-space they do not lead to a change in the physical knot nor an improvement in the quantity under consideration. Theorem 8, therefore, implies that the pivots of breadth one and two are infinitesimal generators of the tangent space of $Equ(n)$ for the generic knot, i.e. one whose vertex set is in “general position.” This implies that in testing for locally optimal configurations, one need only verify that

none of these $2n$ pivots leads to an improvement of the value.

Corollary 11 *A locally optimal value of a spatial knot quantity occurs for a generic knot precisely when none of the $2n$ pivots leads to an improved value.*

The modifications to the above strategy include allowing a random selection of cases that do not improve the optimizing quantity (the simulated annealing strategy) and a strategy in which the movement leading to the better value is amplified and the resulting value tested. The former strategy is designed to help avoid local optima in a search for global optimal values while the latter strategy is analogous to the gradient path method in which one follows the gradient path until a locally optimal value is reached. One recomputes the gradient at this new point and follows the resulting curve in search of next local optimum. Because of the structure of polygonal knot space and the lack of differentiability of the functions being optimized over polygonal knots, we do not pursue the gradient method in this project but employ these various modifications of a random walk instead.

5 Presentation and Analysis of Data

For the energy and ropelength calculations, we focus our attention on equilateral knots composed of 8, 16, and 32 edges. Only 11 knots have been realized as equilateral knots with 8 edges, namely 0.1, 3.1, 4.1, 5.1, 5.2, 6.1, 6.2, 6.3, 8.20, 3.1#3.1, and 3.1#-3.1. These knots compose the population of study for 8 edge knots. Many more knots are realizable with 16 and 32 edges. The knot population for 16 and 32 edge knots includes all knots through 9 crossings. This includes the prime knots and the composite knots 3.1#3.1, 3.1#-3.1, 3.1#4.1, 3.1#5.1, 3.1#-5.1, 3.1#5.2, 3.1#-5.2, 3.1#-6.1, 3.1#-6.1, 3.1#6.2, 3.1#-6.2, 3.1#6.3, 4.1#4.1, 4.1#5.1, 4.1#5.2, 3.1#3.1#3.1, 3.1#3.1#-3.1, a total of 102 knots. The initial conformations for the 8 and 16 edge knots were created by Rob Scharein using KnotPlot [44] and the 32 edge knots were obtained by subdividing each edge of the 16 edge optimized knot. The tables of data in this section consists of the 26 knots that have the lowest calculated ropelength values for 32 edges. The unknot appears to be a highly anomalous case in that the data it provides masks the often highly systematic behavior of the other cases. As a consequence, we have not included the unknot in the data presented and analyzed here. For consistency, we retain the ordering suggested by the 32 edge minimal ropelength values throughout this section. The complete set of data, including vertex coordinates and orderings with respect to the different quantities, are posted at <http://www.math.ucsb.edu/~millet/knotdata.html> and <http://monkey.chatham.edu/~rawdon/knotdata.html>.

In the following subsections, we describe the techniques and exceptional cir-

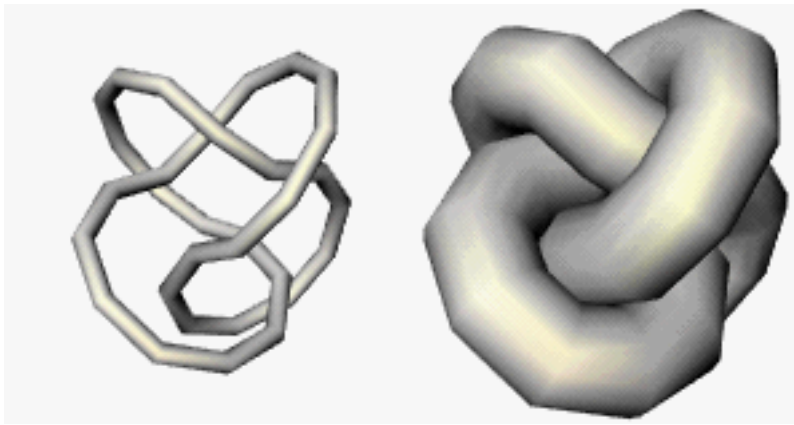


Fig. 4. Figure-8 knots shown with a small tube radius then a tube radius equal to the injectivity radius

cumstances unique to each computation as well as tables and analysis for the data obtained.

5.1 Injectivity Radius, Thickness, and Rope Length

In this section, we describe the computations that find the ropelength-minimized (i.e. thickness-maximized) conformations for the 8, 16, and 32 edge knot populations. Table 1 contains the ropelength and thickness values of these conformations. The method for computing the ropelength of a polygonal knot is described in [29–31]. As mentioned in Section 3, the injectivity radius of a polygonal knot is the minimum of $MinRad(K)$ (minimum radius of curvature) and $\frac{1}{2}DCSD(K)$ (doubly-critical self-distance). For an equilateral knot K , $MinRad(K)$ is the minimum over all vertices v_i of the length of an edge divided by two times the tangent of half the exterior angle at v_i . $MinRad$ measures the minimum over all vertices of the radius of a circular arc that can be inscribed tangentially at the midpoints of adjacent edges. $DCSD$ is the minimum distance between distinct pairs of points that are critical points for the distance function $(x, y) \rightarrow \|x - y\|$. The thickness, $\tau(K)$, is the injectivity radius divided by the length of the knot and the ropelength, $\rho(K)$ is the multiplicative inverse of thickness [29–31]. In Figure 4, we show a 32 edge ropelength-optimized figure-8 knot drawn once with tubes of a small radius to show the shape of the knot and drawn a second time with tube whose radius is the injectivity radius.

Ropelength does not lend itself to a traditional gradient descent. Optimization of the ropelength value is obtained through simulated annealing on random crankshaft rotations (RCR, described in steps 1-4). One step of the algorithm consists of:

- (1) Randomly choose two non-consecutive vertices of the knot K .
- (2) Compute a swivel-angle bound, θ_{max} , so that the topological knot type will not change.
- (3) Choose a random angle θ such that $-\theta_{max} \leq \theta \leq \theta_{max}$.
- (4) Rotate one of the arcs between the two vertices through an angle of θ about the axis passing through the two selected vertices to create a new knot K' of the same knot type.
- (5) If the ropelength of K' is less than the ropelength of K , K' is selected.
- (6) If the ropelength of K' is greater than or equal to the ropelength of K , K' is chosen with a probability of $e^{\frac{\rho_{old} - \rho_{new}}{\rho_{old}} \cdot c}$.

During the process c begins at 10 and is reduced to 2, .8, and .1. The constants were chosen through experimentation in an effort to provide appropriate convergence rates. To theoretically insure that we would find the global minimum of ropelength, a logarithmic reduction in the constant would have to be used [40]. This, however, implied an impractical amount of processing to compute the data for this study. As a result, the knots may not be global minima for the ropelength function.

The knots obtained, however, are local minima up to the maximum reliability of the computer. Using Corollary 11, we can check to see if a knot is a local minimum. $Equ(n)$ is a $2n$ -dimensional manifold (i.e. there are $2n$ tangent directions). A basis of the tangent directions (in the generic case) are the pivots created by rotating about the axis passing through pairs of vertices separated by 1 and 2 vertices. If by completing a rotation at the angle at a low computer tolerance ($\pm .0000000000000001$) for each of these tangent directions, no lower ropelength can be detected, then we can conclude that we are indeed at a local minimum. Using an algorithm derived from this process, we can attempt to find local minima near the knots that appear to be near minima as a result of the simulated annealing process. We begin by selecting a rotation angle of .1 and cycling through all 1 and 2-step pivots of .1 and -.1 until none of these rotations result in an improved ropelength. The angle is then halved and the procedure is repeated until the angle is at the lowest computer tolerance. At the end of this process, we are guaranteed to be at a local minimum up to the maximum reliability of the computer. When the simulated annealing algorithms were completed, this algorithm was applied and each knot was inspected visually using TOROS [45] to insure that the knot was in a position consistent with being a global minimum.

We have observed distinct local minima resulting from different initial conformations. In Figures 5 and 6, we show the initial and final conformations of the original ropelength minimization for the 9.39 knot. Notice that in the original conformation (Figure 5) much of the tangling is concentrated in the small region on the right side of the knot. The simulated annealing process was not able to free those edges although the knot shown is a true local minimum.



Fig. 5. Initial conformation of the 9.39 knot from first optimization attempt, $\rho(K) = 36491.12$

Despite an increase in the constant c and more repetitions, the algorithm was unable to free this tight region (Figure 6). Notice that in the portion of the knot that is not tightly bound, the algorithm made no attempt to expand the knot. This occurs because the ropelength calculation is localized (oftentimes realized as the radius of curvature at only one vertex or the distance between only one pair of critical points of the distance map). The free portion of the knot may or may not change as it need only avoid becoming as tightly bound as the other part. As long as the free portion avoids such tightness, there is no advantage in straightening. As a result, the ropelength surface in knot space will be constant in several of the tangent directions with steep climbs in the remaining directions. This may explain why it is so difficult for the knot to escape from this type of valley.

This behavior is also seen for knots with fewer edges. With the exception of 0.1, 3.1, and 4.1, the 8-edge knot population studied here can be made with a minimum of 8 edges. Thus, the components of $Equ(8)$ corresponding to these knot types are tight and the knots may become stuck in local minima that are different from a global optimal position. The research of Calvo [5] suggests that there may in fact be more than one component of an equilateral knot type that cannot be attributed to translations, rotations, or dihedral actions on the edge numbering. If this is true, initial conformations in separate components will lead to distinct optimal equilateral knots. For 16 and 32 edges, the knots in this study have more freedom within the components and the additional edges provide more potential pivots with which to explore the components. In Figures 7 and 8, we see two different local minima for the 6.3 knot with 8 edges. While it is difficult to determine whether these are two different conformations from the figures alone, the 6.3 knot in Figure 7 has a ropelength of 353.59 while the 6.3 knot from Figure 8 has ropelength of 215.00. This verifies that these

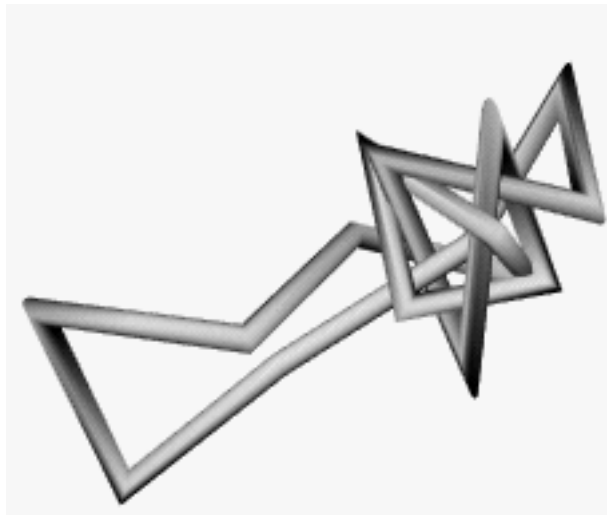


Fig. 6. Local minimum conformation of the 9.39 knot from first optimization attempt, $\rho(K) = 375.71$



Fig. 7. 6.3 knot at a local minimum for ropelength, $\rho(K) = 353.59$

are indeed different equilaterally-equivalent local minima with very different ropelengths.

At the outset of this project, the set of initial conformations were generated by the Monte Carlo samples of $Equ(n)$. Many of these conformations were tightly woven, uneven, and difficult to optimize as seen in Figures 5 and 6. As a consequence, we decided to use another source of initial conformations. These were generated by Rob Scharein using his program KnotPlot [44]. The knots were created by manipulating conformations that minimize a knot energy used in KnotPlot. The program first reduced the number of vertices from between 30-60 (depending on the knot) to 16 while retaining the knot type. Next, two



Fig. 8. 6.3 knot at a local minimum for ropelength, $\rho(K) = 215.00$

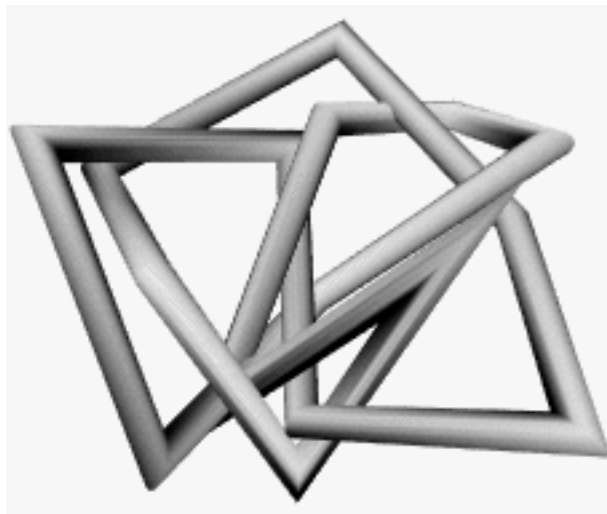


Fig. 9. Scharein's initial conformation of the 9.39 knot from the reported ropelength optimization, $\rho(K) = 779.70$

forces were applied to the knot: one that favors the length of an edge to be 1 and another that guarantees that no edges pass through each other. The knot was randomly perturbed and the forces applied until the ratio of the longest to shortest side was appropriately close to 1. In Figures 9 and 10, we see the initial and final conformations for the 9.39 knot from which the data in this paper is derived. The algorithm has little trouble finding a knot that is much closer to the global minimum from the more regular starting conformation.

We often observe slight differences in the locally minimal values. In Figures 11 and 12, we show the final conformations derived from two different ropelength minimizations of the 32 edge 5.1 knot. The knots appear identical and both have been confirmed to be local minima; however, the ropelength values are

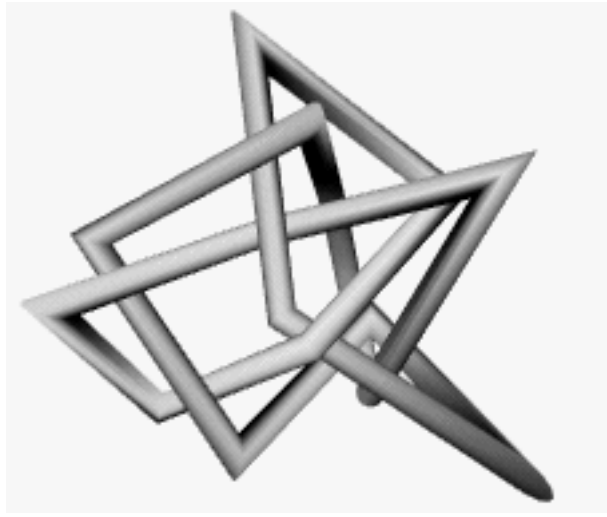


Fig. 10. Ropelength local minimum conformation of the 9.39 knot from the reported ropelength optimization, $\rho(K) = 160.06$

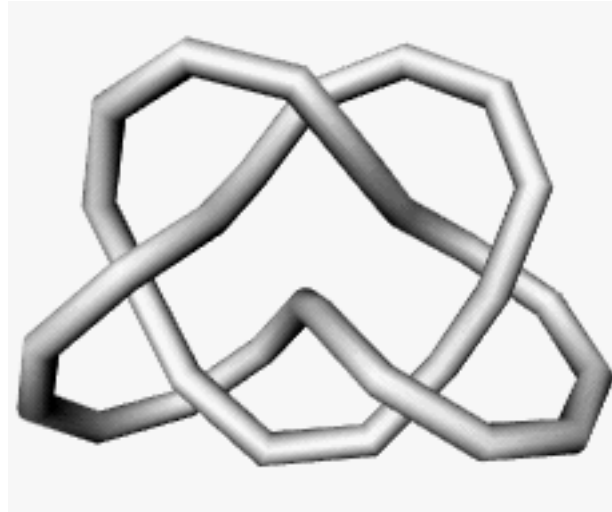


Fig. 11. 32 edge ropelength local minimum 5.1 knot, $\rho(K) = 50.478804$

50.478804 and 50.622445, guaranteeing that these two knots are truly distinct and not the same knot viewed from a different perspective. Other examples of this behavior are common. A slower cooling in the simulated annealing algorithm may make this phenomenon more rare, although we conjecture that the ropelength surface is nearly flat with small dents near a global minimum. If so, it would be easy for the knot to end in a shallow puddle that is near the global minimum but difficult to find a true global minimum. The distinct local minima with similar ropelength values that we have encountered have always been very similar looking knots. For this population with 16 and 32 edges, we have not observed any distinct local minima that appear to be near global minima but are very different looking conformations.

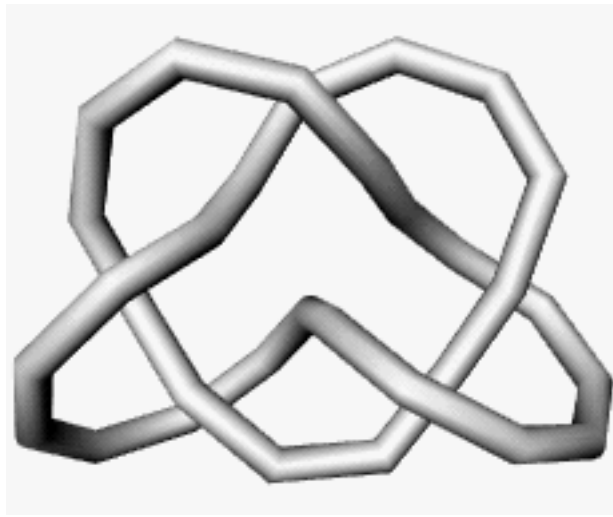


Fig. 12. 32 edge ropelength local minimum 5.1 knot, $\rho(K) = 50.622445$

The results of the optimizations mentioned above are contained in Table 1.

5.2 *Knot Energy*

In this section, we discuss the process of determining the minimum energy of the equilateral knots. The algorithms for optimizing the polygonal version of the Möbius Energy are identical to those explained in Section 5.1 for ropelength and the computation of energy is a straightforward application of dot products and norms. Recall that in this discretization, we approximate half the traditional Möbius Energy. Table 2 contains our estimated minimal energy values for our knot population.

In these energy calculations, we have not been able to achieve global minima. In fact, with the exception of the unknot, none of the conformations are even local minima. The algorithm described in Section 5.1 was employed to search for a local minimum. Slight improvements (on the order of 10^{-3}) were observed during each application of the algorithm. However, these processes failed to converge to a local minimum.

The Möbius Energy is a substantially different quantity compared to ropelength in that it includes interactions between every pair of non adjacent edges. Therefore, one pivot that successfully reduces the energy affects the energy calculations for many of the pairs of edges in the sum. On the other hand, we have observed that the injectivity radius of a knot, is usually realized as half the distance between one particular doubly critical pair or as the radius of curvature at one vertex. Still, there may be many other doubly critical pairs whose distance is close to the injectivity radius or vertices whose radius

Table 1
Ropelength and Thickness of 8, 16, and 32 edge knots

	8 edges		16 edges		32 edges	
Knot	ρ	τ	ρ	τ	ρ	τ
3.1	52.92	0.0189	36.91	0.0271	33.88	0.0295
4.1	108.10	0.0093	49.91	0.0200	43.82	0.0228
5.1	225.50	0.0044	59.99	0.0167	50.48	0.0198
5.2	214.74	0.0047	63.72	0.0157	52.63	0.0190
6.1	258.32	0.0039	77.28	0.0129	61.82	0.0162
3.1#-3.1	257.65	0.0039	75.51	0.0132	61.85	0.0162
3.1#3.1	415.13	0.0024	75.49	0.0132	61.89	0.0162
6.3	215.00	0.0047	80.94	0.0124	63.02	0.0159
6.2	201.29	0.0050	80.73	0.0124	63.74	0.0157
8.19			73.60	0.0136	64.59	0.0155
7.1			90.73	0.0110	68.83	0.0145
8.20	257.24	0.0039	84.40	0.0118	69.30	0.0144
7.3			95.61	0.0105	71.11	0.0141
7.2			92.06	0.0109	71.46	0.0140
7.4			98.01	0.0102	72.32	0.0138
8.21			93.33	0.0107	73.15	0.0137
7.7			105.13	0.0095	73.37	0.0136
3.1#4.1			98.34	0.0102	73.71	0.0136
7.6			103.56	0.0097	74.17	0.0135
7.5			105.07	0.0095	74.45	0.0134
9.46			92.04	0.0109	75.05	0.0133
9.42			95.31	0.0105	76.00	0.0132
9.43			102.31	0.0098	79.72	0.0125
9.44			110.67	0.0090	80.03	0.0125
3.1#-5.1			111.03	0.0090	81.16	0.0123
8.3			116.95	0.0086	81.62	0.0123
8.1			117.68	0.0085	81.65	0.0122

of curvature is close to the injectivity radius. To reduce the ropelength, the injectivity radius realizing value must be increased without disturbing any of the other values. If a knot is near a local minimum, very few pivots are likely to do this. Thus, compared to ropelength, there are many more pivots that could reduce the Möbius energy.

Still, we were able to test the criticality of the equilateral knots by using the program Ming, written by Ying-Qing Wu [46]. Ming uses a gradient-type flow to find energy minima for knots in $Geo(n)$. Upon completing the simulated annealing in $Equ(n)$, the knots were imported into Ming and the gradient descent algorithm applied. Little improvement was observed for any of the knots. Since the gradient-type descent works in $Geo(n)$, some improvement will always occur because the tension to keep the knot equilateral has been released. Because little improvement occurred using Ming, we believe that each knot is very close to a global equilateral energy minimum. In the case of $Geo(n)$, many distinct local energy minima have been found by J. Simon and J. Tockle [47] using Ming. As above, other examples of local minima with similar energies are common, but no pair of very different looking global minimal conformations have been found. Thus, it appears that the energy surface in $Geo(n)$ is also nearly constant yet dented near a global minimum.

The result of the energy minimization process applied to the 16 edge 9.39 knot from Figure 5 is shown in Figure 13. Notice that the energy minimization algorithm was unable to loosen the tight region of the knot as was also the case for ropelength. However, the more global nature of the energy forces the “free” portion of the knot to become more circle-like to minimize the self-interactions of the edges in this region. Thus, the energy surface is not constant in directions related to moving the free portion as in the case of ropelength but is rather gently sloping towards this final conformation. Still, the steep cliffs in the remaining directions make it difficult for the knot to find even more relaxed conformations. Figure 14 shows the energy-minimizing conformation from the initial conformation of Scharein that is reported in this paper. We note that the 9.39 conformation in Figure 14 has box length 13.81 while that in Figure 10 has box length 12.65, proving that the energy and ropelength optima are distinct conformations.

The results of the energy optimizations mentioned above are contained in Table 2.

5.3 Average Crossing Number, Average Writhe, and Total Curvature

In this section, we present the average crossing number (ACN), average writhe (AW), and total curvature (TC) for ropelength and energy optimized equilat-

Table 2
Minimal E_{MD} of 8, 16, and 32 edge knots

	Minimal E_{MD}		
Knot	8 edges	16 edges	32 edges
3.1	103.91	50.59	41.31
4.1	377.79	90.38	66.87
5.1	1316.28	122.05	83.41
5.2	1311.58	136.42	91.80
6.1	1972.22	197.95	118.42
3.1#-3.1	2525.21	178.93	108.33
3.1#3.1	6292.12	177.78	108.26
6.3	1443.26	217.05	130.35
6.2	1238.93	201.32	124.56
8.19		211.00	141.68
7.1		263.19	134.81
8.20	2504.14	245.85	153.70
7.3		278.32	151.59
7.2		311.33	147.69
7.4		284.14	157.13
8.21		289.59	164.98
7.7		320.32	164.91
3.1#4.1		290.81	146.43
7.6		326.74	164.96
7.5		331.27	160.51
9.46		313.15	185.84
9.42		313.24	183.99
9.43		364.39	194.93
9.44		419.96	199.35
3.1#-5.1		372.98	172.64
8.3		436.98	187.18
8.1		397.15	181.13

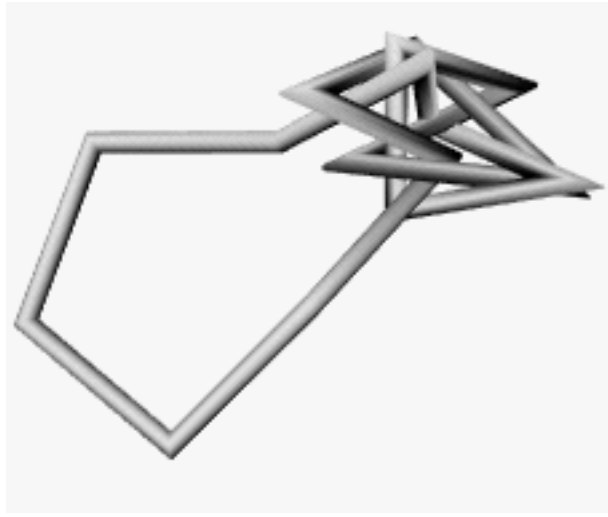


Fig. 13. Energy local minimum conformation of the 9.39 knot from first optimization attempt, $E(K) = 2389.12$

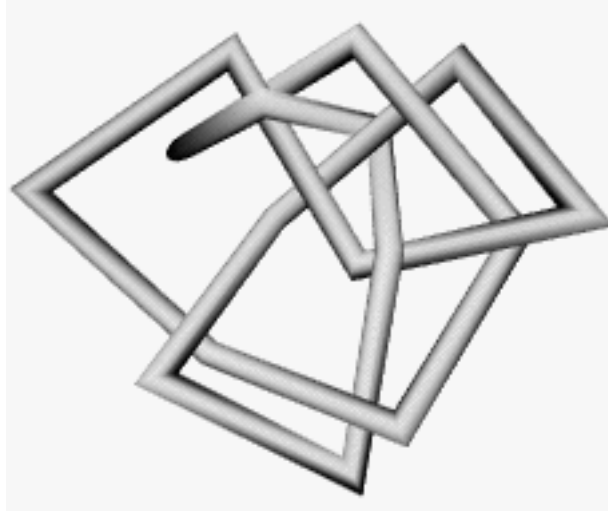


Fig. 14. Energy local minimum conformation of the 9.39 knot from the reported optimization, $E(K) = 748.09$

eral knots of 8, 16, and 32 edges. The average crossing number of a knot conformation is the average over all viewing directions of the number of observed crossings as described in Section 3. For a polygonal knot conformation, the average crossing number can be computed in closed form as a function of the vertices via an algorithm derived by T. Banchoff [48]. The average writhe can be determined by a similar computation in which the signed crossings are averaged. Since we make no distinction in this paper between mirror images, we report the absolute values of the average writhes determined by our computations. The total curvature of a polygonal knot conformation is the sum of the exterior angles at the vertices. The computed values are contained in

Table 3
8 edge optimized knots: ACN, AW, TC

	8 edges					
	E -minimized			ρ -minimized		
Knot	ACN	AW	TC	ACN	AW	TC
3.1	4.69	3.30	14.48	4.65	3.32	14.58
4.1	7.52	0.07	17.37	7.56	0.10	17.47
5.1	9.84	5.80	19.28	10.28	5.95	19.36
5.2	9.69	4.98	18.84	9.77	4.96	18.87
6.1	10.80	1.12	20.08	11.02	1.05	20.28
3.1#-3.1	14.28	0.03	20.06	14.31	0.03	20.02
3.1#3.1	13.78	6.54	19.89	13.76	6.53	19.77
6.3	11.92	0.22	19.51	12.06	0.19	19.54
6.2	11.03	2.31	18.95	11.20	2.29	19.00
8.20	14.18	2.04	20.11	14.20	2.04	20.07

Tables 3, 4, and 5.

5.4 Box Dimensions of Knots

In this section, we present the values for the box length (BL), box width (BW), box height (BH), box volume (BV), and box surface area (BSA) (defined in Section 3) for ropelength and energy optimized equilateral knots of 8, 16, and 32 edges. In these calculations, the length of the knot has been set to 100, in order to better display the relative values. The computed values are contained in Tables 6-11.

5.5 Surface Area and Volume of Convex Hulls

In this section, we present values for the convex hull volume (HV) and surface area (HSA) for ropelength and energy optimized equilateral knots of 8, 16, and 32 edges. The convex hulls were established by finding the triplets of vertices that determine bounding planes for the polyhedron. The sum of the areas of the triangles related to these triplets is the surface area. Each triplet with the addition of the center point of the knot (the average of the coordinates of the vertices) determines a pyramid; the sum of the volumes of these pyramids is

Table 4

16 edge optimized knots: ACN, AW, TC

	16 edges					
	E -minimized			ρ -minimized		
Knot	ACN	AW	TC	ACN	AW	TC
3.1	4.24	3.34	14.64	4.42	3.36	15.09
4.1	6.16	0.00	16.96	6.66	0.00	17.51
5.1	7.44	5.88	19.79	7.86	6.13	20.41
5.2	7.88	4.72	19.62	8.38	4.60	20.25
6.1	10.09	1.31	21.86	10.81	1.18	21.97
3.1#-3.1	9.35	0.00	22.79	10.02	0.01	23.03
3.1#3.1	9.71	6.66	22.60	10.58	6.70	22.98
6.3	10.71	0.17	23.15	11.55	0.00	22.32
6.2	10.39	2.46	22.97	11.01	2.50	23.82
8.19	10.90	8.41	21.02	11.26	8.39	21.03
7.1	11.50	8.54	24.28	12.50	8.83	25.59
8.20	11.75	2.09	22.42	12.84	2.16	21.98
7.3	11.75	7.33	23.90	13.69	7.40	24.56
7.2	12.71	6.33	26.30	13.15	5.76	25.06
7.4	12.31	6.30	24.17	12.92	6.14	25.11
8.21	12.62	4.61	23.23	13.25	4.77	23.59
7.7	12.48	0.86	24.55	14.10	1.11	26.55
3.1#4.1	12.15	3.35	25.06	13.02	3.46	25.59
7.6	13.29	3.04	25.85	14.83	3.15	25.69
7.5	13.88	7.62	25.72	15.40	7.41	26.33
9.46	13.57	2.96	22.78	14.20	2.92	23.95
9.42	13.62	1.10	23.58	14.08	1.04	24.60
9.43	14.67	5.25	24.97	15.22	5.23	26.07
9.44	15.22	1.26	25.90	15.57	1.25	25.14
3.1#-5.1	13.87	2.76	27.02	14.83	2.79	28.07
8.3	14.57	0.03	25.88	18.84	0.18	29.53
8.1	14.41	2.70	27.17	18.00	2.40	27.7

Table 5
32 edge optimized knots: ACN, AW, TC

	32 edges					
	E -minimized			ρ -minimized		
Knot	ACN	AW	TC	ACN	AW	TC
3.1	4.18	3.35	14.66	4.30	3.38	16.59
4.1	6.10	0.00	17.41	6.57	0.01	20.54
5.1	7.27	5.88	21.23	7.89	6.19	23.13
5.2	7.76	4.71	20.29	8.35	4.60	22.58
6.1	9.28	1.45	23.72	10.29	1.20	25.03
3.1#-3.1	8.29	0.00	23.37	9.58	0.00	26.07
3.1#3.1	8.37	6.70	23.38	9.55	6.73	25.58
6.3	9.85	0.03	22.20	10.77	0.01	25.98
6.2	9.57	2.61	23.00	10.71	2.71	26.54
8.19	10.54	8.44	21.35	10.60	8.42	21.92
7.1	10.27	8.30	28.40	11.79	8.98	29.67
8.20	11.06	2.08	23.60	12.15	2.07	23.66
7.3	10.98	7.22	25.65	12.07	7.42	27.47
7.2	10.80	6.23	27.28	12.21	5.79	27.83
7.4	11.21	6.12	25.84	12.37	5.83	27.40
8.21	11.55	4.62	23.91	12.95	4.68	25.83
7.7	11.51	3.18	26.29	13.13	0.64	27.47
3.1#4.1	10.32	3.36	26.49	12.60	3.37	27.65
7.6	11.52	3.24	26.18	13.02	3.35	27.94
7.5	11.34	7.35	26.02	12.88	7.31	29.02
9.46	12.74	2.89	24.33	13.33	2.96	24.82
9.42	12.62	1.11	24.38	13.55	1.10	25.93
9.43	12.88	5.23	25.47	13.97	5.31	27.10
9.44	13.22	1.42	25.89	14.58	1.41	27.64
3.1#-5.1	11.56	2.50	29.66	13.25	2.80	31.14
8.3	12.67	0.02	28.27	14.16	0.01	30.13
8.1	12.44	3.00	30.41	14.54	2.32	30.61

Table 6

Box dimensions for 8 edge energy-minimized knots (Length = 100)

	8 edge E -minimized				
Knot	BL	BW	BH	BV	BSA
3.1	22.12	11.57	11.01	2816.73	1253.47
4.1	19.45	14.82	9.74	2808.54	1244.41
5.1	16.07	13.53	11.80	2566.75	1133.74
5.2	15.18	13.83	11.91	2498.87	1110.45
6.1	15.62	14.33	9.40	2104.83	1011.00
3.1#-3.1	12.50	12.42	12.27	1904.46	921.89
3.1#3.1	12.76	12.50	8.56	1364.55	751.18
6.3	13.92	12.47	11.23	1949.18	939.82
6.2	14.85	12.40	10.89	2005.67	961.91
8.20	12.50	12.50	11.86	1853.67	905.67

Table 7

Box dimensions for 8 edge ropelength-minimized knots (Length = 100)

	8 edge ρ -minimized				
Knot	BL	BW	BH	BV	BSA
3.1	20.37	12.54	10.94	2794.36	1230.92
4.1	19.85	14.25	9.05	2559.42	1182.80
5.1	15.07	13.71	12.03	2485.45	1105.65
5.2	15.07	13.83	12.02	2505.14	1111.56
6.1	15.10	14.09	9.30	1979.77	968.79
3.1#-3.1	12.50	12.45	12.26	1908.78	923.29
3.1#3.1	12.75	12.49	8.71	1386.43	757.97
6.3	13.91	12.70	10.47	1850.10	910.69
6.2	14.70	12.41	10.44	1903.33	930.52
8.20	12.50	12.50	11.93	1863.33	908.77

the volume of the convex hull. In these calculations, the length of the knot has been set to 100 to better display the relative values. The computed values are contained in Tables 12, 13, and 14.

Table 8

Box dimensions for 16 edge energy-minimized knots (Length = 100)

	16 edge E -minimized				
Knot	BL	BW	BH	BV	BSA
3.1	19.26	17.33	11.95	3987.93	1541.92
4.1	16.30	14.25	13.47	3129.60	1287.79
5.1	17.43	11.98	10.72	2239.82	1048.60
5.2	16.92	14.29	13.18	3186.56	1306.23
6.1	15.22	14.22	10.81	2340.66	1069.68
3.1#-3.1	16.74	12.44	7.33	1525.05	843.76
3.1#3.1	18.74	12.95	9.29	2254.75	1074.28
6.3	16.75	14.08	6.39	1506.42	865.40
6.2	18.88	12.74	5.83	1402.18	849.68
8.19	15.82	13.74	8.18	1778.45	918.37
7.1	15.83	14.44	6.54	1494.80	853.15
8.20	14.28	11.45	10.98	1795.62	892.16
7.3	20.38	7.78	6.09	965.89	660.22
7.2	16.44	10.35	8.96	1523.21	819.92
7.4	17.21	9.15	6.57	1035.10	661.53
8.21	14.08	11.40	11.14	1787.10	888.38
7.7	15.85	9.67	5.79	886.60	601.71
3.1#4.1	15.15	12.00	9.82	1785.33	896.84
7.6	14.94	11.55	6.99	1206.55	715.56
7.5	16.57	11.17	6.49	1201.60	730.35
9.46	12.94	11.75	10.51	1596.98	822.74
9.42	12.19	11.91	11.54	1676.62	847.00
9.43	12.57	12.37	7.01	1089.67	660.57
9.44	15.26	12.05	6.16	1132.77	704.24
3.1#-5.1	15.24	13.03	8.02	1592.04	850.42
8.3	19.86	6.76	6.64	891.37	621.99
8.1	17.92	9.44	8.43	1425.83	799.57

Table 9

Box dimensions for 16 edge ropelength-minimized knots (Length = 100)

	16 edge ρ -minimized				
Knot	BL	BW	BH	BV	BSA
3.1	18.55	17.24	12.17	3890.73	1510.41
4.1	15.12	14.02	13.05	2765.53	1184.28
5.1	16.20	11.79	11.02	2104.32	998.74
5.2	17.40	12.94	10.03	2259.71	1059.38
6.1	14.34	13.25	10.95	2080.68	984.25
3.1#-3.1	14.70	12.67	10.37	1930.64	939.93
3.1#3.1	17.14	12.00	8.80	1809.49	924.02
6.3	14.52	12.27	11.61	2068.43	978.39
6.2	18.00	14.72	5.67	1501.46	900.66
8.19	15.37	13.27	8.76	1785.09	909.16
7.1	15.92	13.49	8.45	1815.94	926.94
8.20	12.81	11.41	11.11	1623.19	830.27
7.3	13.66	11.09	10.76	1629.83	835.55
7.2	14.81	10.59	10.07	1579.73	825.32
7.4	16.68	13.71	6.74	1539.92	866.55
8.21	15.14	12.02	10.39	1890.76	928.31
7.7	14.94	10.28	8.20	1258.98	720.65
3.1#4.1	15.56	13.57	8.53	1802.48	919.73
7.6	12.72	10.64	8.32	1125.63	659.22
7.5	13.20	11.07	10.00	1461.51	777.77
9.46	13.05	11.63	10.27	1558.00	810.24
9.42	14.63	12.58	8.91	1639.76	852.93
9.43	13.32	9.79	8.53	1112.73	655.20
9.44	13.96	11.50	8.77	1407.82	767.62
3.1#-5.1	13.61	12.69	7.05	1217.21	716.09
8.3	13.56	10.24	7.49	1039.26	633.94
8.1	13.84	7.84	6.73	729.59	508.54

Table 10

Box dimensions for 32 edge energy-minimized knots (Length = 100)

	32 edge E -minimized				
Knot	BL	BW	BH	BV	BSA
3.1	18.83	17.70	11.73	3907.69	1523.16
4.1	16.11	14.28	13.69	3148.86	1292.02
5.1	16.39	15.35	6.62	1665.69	923.54
5.2	16.84	13.39	11.43	2576.76	1141.89
6.1	15.87	12.18	10.06	1943.44	950.59
3.1#-3.1	19.58	13.01	6.34	1614.41	922.60
3.1#3.1	19.44	10.71	8.13	1693.72	907.03
6.3	14.97	11.64	9.80	1707.65	870.06
6.2	15.63	11.96	8.93	1670.09	866.86
8.19	14.34	13.98	8.51	1706.05	882.96
7.1	15.72	15.26	4.29	1027.69	745.06
8.20	15.70	12.08	8.16	1547.35	832.58
7.3	16.86	10.91	9.44	1735.80	892.00
7.2	15.98	11.81	8.26	1559.85	836.85
7.4	16.19	10.66	9.35	1612.77	846.99
8.21	14.13	13.60	8.41	1615.85	850.59
7.7	14.48	12.04	7.65	1333.98	754.56
3.1#4.1	18.42	11.21	8.35	1724.88	908.06
7.6	13.70	11.72	9.81	1574.12	819.54
7.5	14.88	10.48	10.40	1620.84	839.06
9.46	14.48	10.74	9.43	1467.32	786.96
9.42	13.73	12.49	9.07	1554.73	818.40
9.43	13.88	11.33	10.03	1577.28	820.21
9.44	13.73	11.30	9.13	1416.42	767.27
3.1#-5.1	18.49	10.78	5.04	1004.71	693.87
8.3	16.34	9.73	8.95	1422.52	784.47
8.1	15.66	11.89	7.29	1357.59	774.20

Table 11

Box dimensions for 32 edge ropelength-minimized knots (Length = 100)

	32 edge ρ -minimized				
Knot	BL	BW	BH	BV	BSA
3.1	18.41	17.17	10.44	3300.02	1375.07
4.1	14.51	14.03	13.70	2788.78	1189.09
5.1	16.58	11.95	10.13	2008.15	974.60
5.2	16.09	11.89	10.50	2009.04	970.27
6.1	14.88	13.06	8.05	1564.18	838.40
3.1#-3.1	17.52	13.35	6.44	1507.68	865.89
3.1#3.1	17.58	10.04	8.39	1479.20	815.88
6.3	13.64	13.00	9.58	1700.26	865.57
6.2	13.90	11.87	9.82	1621.07	836.40
8.19	14.37	13.96	8.27	1657.98	869.40
7.1	15.12	11.89	7.31	1314.25	754.45
8.20	14.08	11.71	10.29	1697.56	860.86
7.3	15.62	10.33	8.84	1426.42	781.53
7.2	15.26	9.78	8.77	1309.21	737.81
7.4	14.73	10.66	8.38	1315.60	739.51
8.21	13.03	11.19	9.83	1432.81	767.63
7.7	12.26	11.32	10.92	1514.44	792.19
3.1#4.1	13.83	10.69	10.35	1530.37	803.33
7.6	14.37	10.46	10.25	1540.18	809.46
7.5	14.53	10.32	9.15	1372.65	754.88
9.46	13.29	11.45	11.14	1693.48	854.97
9.42	12.74	11.94	10.70	1627.47	832.32
9.43	13.28	12.61	9.35	1566.34	819.26
9.44	11.33	11.26	10.27	1309.43	718.87
3.1#-5.1	15.83	10.17	6.87	1106.31	679.39
8.3	14.49	10.33	7.49	1120.87	671.01
8.1	13.15	11.28	7.95	1179.06	685.02

Table 12

Convex hull volume and surface area for 8 edge optimized knots (Length = 100)

	8 edges			
	E -minimized		ρ -minimized	
Knot	HV	HSA	HV	HSA
3.1	865.27	545.12	851.98	543.59
4.1	663.47	452.78	613.40	441.84
5.1	576.24	395.18	558.41	389.64
5.2	562.46	400.16	557.96	398.51
6.1	475.85	357.25	448.85	345.69
3.1#-3.1	491.70	351.47	492.54	351.77
3.1#3.1	364.31	313.46	367.98	315.41
6.3	469.15	361.65	452.02	355.97
6.2	472.55	365.63	449.95	355.63
8.20	493.62	350.03	495.33	350.91

5.6 Numerical Estimation of Knot Probabilities

If an equilateral polygon is selected at random, what is the probability that it will represent a specified topological knot type? Equivalently, what proportion of equilateral knot space consists of knots of this type. This data is an update of that provided in [8], [13], and [14].

The knot probabilities are estimated by means of a Metropolis Monte Carlo sampling method. The basic operation is the random selection of a pair of vertices of the equilateral polygon and the random selection an angle of rotation for which there are no constraints imposed. A rotation of this angle is applied to the segment of the polygonal configuration lying between the two designated vertices about the axis they define. This algorithm is known to generate an example of every equilateral knot conformation, [8]. This operation is applied sequentially and the results are selected randomly or according to fixed criteria, e.g. every 10th step, to define the knot population sample. In this project, we have studied the populations consisting of equilateral polygons with 8, 16 and, 32 edges.

For the purposes of this project, the coordinates of the vertices of the knot are reported as well as a carefully constructed expression of the crossing data. The first provides the initial data used in our first attempts to study the physical knot quantities and the second provides a reconstitution of the knot of the

Table 13

Convex hull volume and surface area for 16 edge optimized knots (Length = 100)

	16 edges			
	E -minimized		ρ -minimized	
Knot	HV	HSA	HV	HSA
3.1	1131.84	637.56	1130.11	616.19
4.1	840.06	512.82	859.46	493.65
5.1	597.16	438.02	605.67	423.63
5.2	665.00	435.25	593.37	408.41
6.1	509.81	371.04	506.07	359.31
3.1#-3.1	526.32	387.04	474.75	351.51
3.1#3.1	541.62	385.99	457.54	343.26
6.3	441.93	346.24	484.89	342.36
6.2	442.58	362.59	410.89	355.70
8.19	525.95	364.52	516.84	358.44
7.1	409.37	333.02	415.96	326.23
8.20	451.18	336.36	489.03	337.10
7.3	331.33	297.07	403.51	312.73
7.2	401.08	327.10	404.53	316.48
7.4	403.13	334.61	398.57	346.68
8.21	431.56	320.50	419.23	323.76
7.7	380.25	328.73	335.85	291.36
3.1#4.1	480.88	347.19	408.52	327.55
7.6	430.68	338.76	370.69	293.46
7.5	376.02	299.36	329.12	271.27
9.46	371.61	298.40	403.58	301.03
9.42	391.60	300.75	377.97	307.23
9.43	375.14	287.93	351.34	281.68
9.44	342.12	293.66	339.73	276.34
3.1#-5.1	401.01	321.54	352.05	296.93
8.3	305.09	281.36	269.51	242.89
8.1	355.99	301.88	248.44	229.71

Table 14

Convex hull volume and surface area for 32 edge optimized knots (Length = 100)

	32 edges			
	E -minimized		ρ -minimized	
Knot	HV	HSA	HV	HSA
3.1	1154.62	643.95	1047.8	613.61
4.1	904.97	532.83	836.29	490.16
5.1	657.91	480.41	680.30	444.92
5.2	757.49	465.16	677.15	425.47
6.1	636.33	419.12	556.24	378.58
3.1#-3.1	642.16	470.75	517.57	390.56
3.1#3.1	648.75	467.39	576.58	396.99
6.3	602.77	393.47	532.53	353.73
6.2	611.13	407.35	523.44	354.02
8.19	584.83	385.72	538.29	369.91
7.1	491.64	404.75	474.48	345.43
8.20	515.18	366.76	487.92	335.72
7.3	528.17	374.43	465.42	342.53
7.2	524.05	380.11	449.27	333.85
7.4	507.54	365.54	450.50	329.49
8.21	488.25	361.09	448.35	318.04
7.7	500.44	357.68	441.65	310.95
3.1#4.1	567.93	407.64	456.00	324.27
7.6	510.96	355.48	435.21	315.40
7.5	526.85	365.13	429.19	315.09
9.46	463.93	337.58	440.18	319.50
9.42	469.13	337.28	449.22	317.90
9.43	452.02	332.55	404.09	304.25
9.44	447.73	328.78	402.70	293.09
3.1#-5.1	409.66	365.72	393.60	324.47
8.3	452.41	342.91	411.26	314.03
8.1	469.38	352.83	398.97	300.62

same topological knot type. This crossing data is analyzed by means of the HOMFLY knot invariant program developed by Ewing and Millett [49]. The HOMFLY polynomial [41,42] has integer coefficients and has as variables L and M and their formal inverses. While the calculation of the HOMFLY polynomial is known to be an exponentially difficult problem, [50], its calculation in this population has proved to be exceptionally fast and, therefore, provides an excellent research tool for this study. Indeed, based upon these calculations, one might conjecture that the calculation of the HOMFLY polynomial of a random polygonal knot has polynomial complexity with probability one.

Since the HOMFLY polynomial is not a faithful detector of the topological knot type, i.e. two distinct topological knots may have equal HOMFLY polynomials, the data used in this study is only an estimation of the knot population. Jim Hoste [51] reports that for the 2,092,241 topological knot types, with minimal crossing representations of no more than sixteen crossings, there are 1,471,651 distinct HOMFLY polynomials. For those with no more than twelve crossings, the HOMFLY polynomial is more than 90% faithful. For the population of knots in $Equ(16)$, the foundation of this study, the HOMFLY polynomial appears to be an effective identifier of the knot type. As a consequence, the fraction of occurrences of the corresponding HOMFLY polynomial of the associated topological knot type provides an effective provisional estimate of the knot population.

Thus, the knot probabilities are actually estimations of the occurrences of the corresponding HOMFLY knot polynomial given by the ratio of the number of occurrences of the HOMFLY polynomial of the topological knot type to the total size of the sample. In a very few cases, we have studied the convergence of these estimates as the size of the sample increases. This has been the principal method of assessing the quality of the estimate and providing a more accurate estimate of the actual number of knot types and their relative frequency, see [8] or [13].

6 Comparison of Physical Knot Parameters

In addition to a desire to carefully explore the relationship between energy and ropelength over a large class of knots, an underlying motivation for undertaking the collection of this data is the search for unforeseen relationships among physical knot parameters and other artifacts of geometric and statistical knot theory. One example is the discovery and use of fundamental quantities as a means to define or measure notions of complexity of knots. Another example is to determine how well these notions correlate with experimental measures of knot complexity such as the flow of DNA knots in gel electrophoresis. Do these various measure reflect the same information or do they capture independent

Table 15
Probabilities for 8, 16, and 32 edge knots

Knot	Probability		
	8 edges	16 edges	32 edges
3.1	0.00956010	0.06438900	0.05611080
4.1	0.00030110	0.01834750	0.00859033
5.1	0.00000223	0.00734240	0.00189590
5.2	0.00000444	0.01261630	0.00318695
6.1	0.00000042	0.00353423	0.00054377
3.1#-3.1	0.00000000	0.00125110	0.00044837
3.1#3.1	0.00000000	0.00117194	0.00045766
6.3	0.00000122	0.00287812	0.00031712
6.2	0.00000133	0.00464800	0.00061129
8.19		0.00069403	0.00005159
7.1		0.00039359	0.00004343
8.20	0.00000000	0.00148048	0.00011114
7.3		0.00035972	0.00004742
7.2		0.00084646	0.00009521
7.4		0.00048969	0.00004931
8.21		0.00090353	0.00006562
7.7		0.00078682	0.00005709
3.1#4.1		0.00088107	0.00021641
7.6		0.00140611	0.00012404
7.5		0.00106995	0.00009692
9.46		0.00018446	0.00001612
9.42		0.00048233	0.00002788
9.43		0.00024963	0.00002238
9.44		0.00049227	0.00002560
3.1#-5.1		0.00009426	0.00002257
8.3		0.00005965	0.00000436
8.1		0.00015722	0.00000872

dimensions of knot complexity?

The data presented in the previous section concerns knots that have been optimized with respect to either ropelength or energy. Some of the relationships involving these quantities, that we will discuss in this section, have been developed in the work of other researchers. For example, Freedman, et al. have given a bound relating the energy and the average crossing number [19]. Buck, Rawdon, and Simon [52] have explored the relationship between the energy and the ropelength. Stasiak, et al. [2] have studied the relationship between another definition of ropelength, the average writhe, the average crossing number, gel speed, etc., for knots with a large number of edges.

6.1 *Energy, Ropelength, and Average Crossing Numbers*

Freedman, He, and Wang [19] show that the average crossing number of a knot is bounded by the energy of the knot divided by 2π . Buck, Rawdon, and Simon [52] show that the energy of the knot is bounded by 4.63 times the $4/3$ power of the ropelength implying a $4/3$ power bound of the average crossing number by the ropelength. In his March 19, 1998 letter to Nature [53], Buck describes the reasons why this $4/3$ power law bound of the average crossing number of a knot by its ropelength can not be improved. Following up on earlier work [1–3] with simple knots suggesting a linear relationship between the average crossing number and the ropelength, Stasiak, Dubochet, Katritch, and Pieranski [4] have explored this relationship between $(2, n)$ torus knots for $3 \leq n \leq 63$. This data shows that the rate of growth of the relation increases with increasing number to twists. Pieranski [54] has further studied the relationship between the average crossing number and the ropelength by considering prime knots through nine crossings and observes that the relationship, “apparently linear at the beginning, is clearly nonlinear in the larger interval.”

In this project, we have added the composite knots to the population. Let $K_{\rho n}$ denote the equilateral n -edge ropelength optimized knot. Similarly, K_{En} will denote an equilateral n -edge E_{MD} optimized knot. The relationship between the ropelength and the average crossing number of the knot is approximately linear, as is shown graphically in Figure 15. This relationship is given by the formula:

$$Equ(32) : ACN(K_{\rho 32}) = -3.14 + 0.22 \rho(K_{\rho 32}), R^2 = 0.97 .$$

The energy is bounded by $4/3$ power of ropelength according to [52]. To test this relationship we have fitted a $4/3$ power equation to this data as follows:

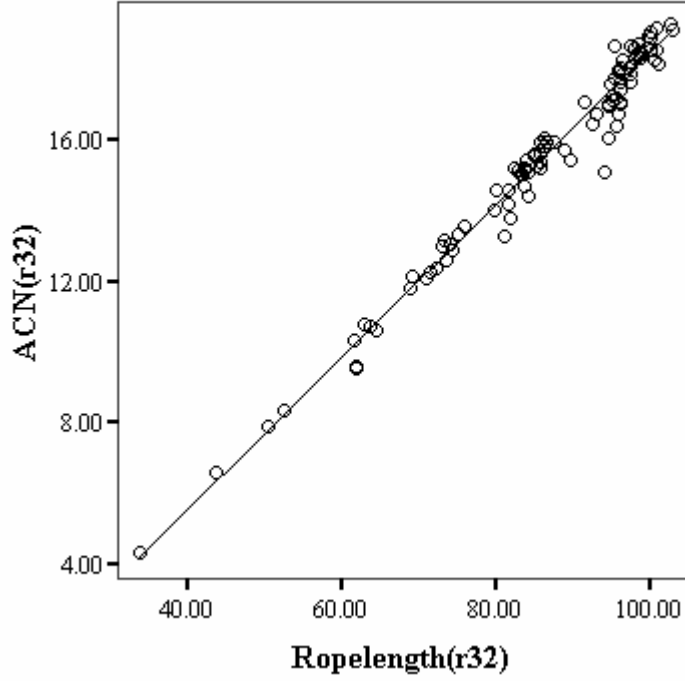


Fig. 15. $ACN(K_{\rho 32})$ versus $\rho(K_{\rho 32})$

$$Equ(32) : E_{MD}(K_{\rho 32}) = -81.94 + 0.89 \rho(K_{\rho 32})^{4/3}, \quad R^2 = 0.97.$$

This data is shown in Figure 16. This suggests that the bound actually provides an excellent approximation to the relationship between the data.

Thus, these apparent relationships suggest a 3/4 power law relationship between energy and average crossing number. This data is shown in Figure 17. The relationship is expressed by the following equation:

$$Equ(32) : ACN(K_{\rho 32}) = 1.55 + 0.22 E_{MD}(K_{\rho 32})^{3/4}, \quad R^2 = 0.99.$$

Finally, since it appears that there may be spatial differences between energy and ropelength optimized knots of the same type, we tested the correlation between the average crossing numbers and the energy of the 32-edge energy optimized knots. This data is shown in Figure 18. The relationship is expressed by the following equation:

$$Equ(32) : ACN(K_{E32}) = 0.99 + 0.23 E_{MD}(K_{E32})^{3/4}, \quad R^2 = 0.99.$$

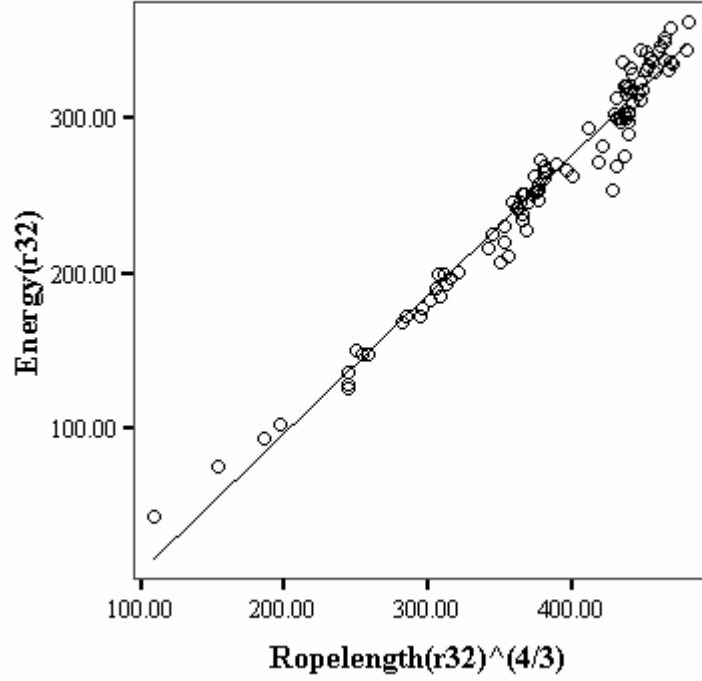


Fig. 16. $E_{MD}(K_{\rho 32})$ versus $\rho(K_{\rho 32})^{4/3}$

This provides further evidence that the bound actually provides an excellent approximation to the relationship between the data.

6.2 Comparison of Ropelength and Energy Optimized Knot Conformations

Earlier, we mentioned that the ropelength and candidate energy optimized conformations are distinct despite some visual similarities. In this section we discuss the similarity and difference between the corresponding optimizations of knots in our population.

In Figures 11 and 12 on page 23, we see two ropelength local minima of the 32 edge 5.1 knot. The conformations appear very similar. The energy minimizing conformation for the 32 edge 5.1 knot is shown in Figure 19. Notice that the shape of this conformation is much different. The energy minimizing conformation exposes more of the symmetries of the knot, while the ropelength minimizing conformation attempts to efficiently consume as much of the space about the knot as possible. Despite the differences between the two functions and between their optima, some spatial measures of the optima are surprisingly similar.

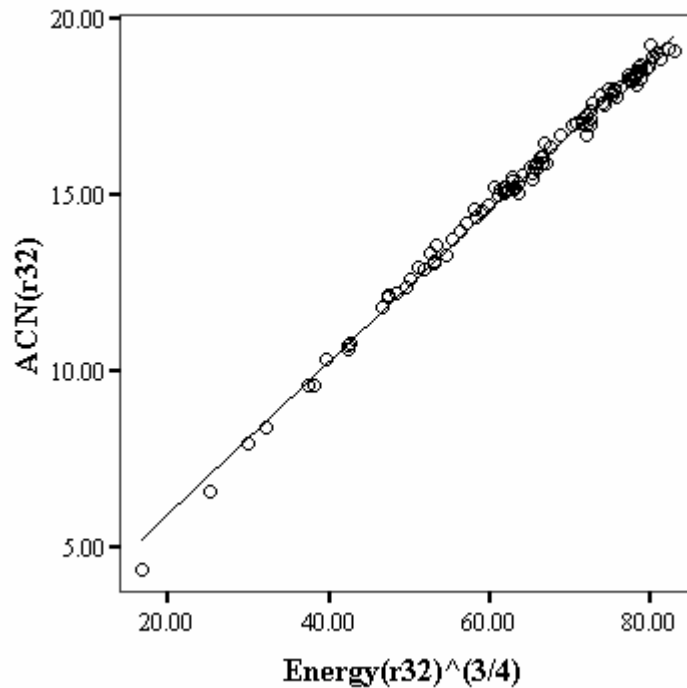


Fig. 17. $ACN(K_{\rho 32})$ versus $E_{MD}(K_{\rho 32})^{3/4}$

For example, the difference in the average crossing numbers as expressed by the equation:

$$Equ(32) : ACN(K_{E32}) = 1.35 + 0.77 ACN(K_{\rho 32}), \quad R^2 = 0.95 .$$

6.3 Probability, Ropelength and, Energy

In Sections 2 and 3 we have discussed the relationship between $\mu(K)$, the existence of embedded tubes with the knot K as its core, the ropelength, and thickness. When the thickness is smaller than the edge length, $\mu(K)$ provides the dominant contribution to the thickness and connects thickness to the radius of a neighborhood of the knot in $Equ_0(n)$ that lies entirely within the component containing K . In this regime, a configuration of optimal thickness lies in the largest region of the component defining the equilateral knot type. Its size, one might postulate, should provide an indicator of the relative size of the component in knot spaces as measured by the proportion of knot space it defines. As a rough approximation, if the components are quite concentrated about the optimal ropelength knot, there should be a correlation

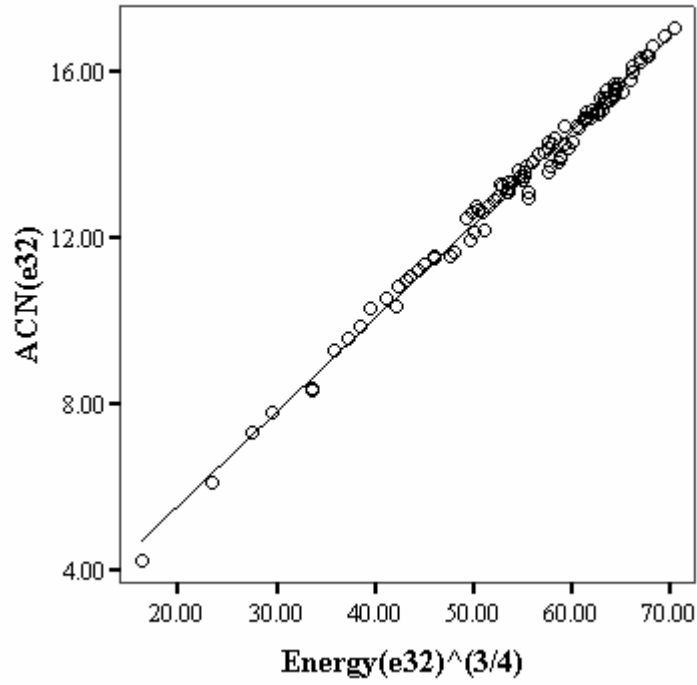


Fig. 18. $ACN(K_{E32})$ versus $E_{MD}(K_{E32})^{3/4}$



Fig. 19. 32 edge energy local minimum 5.1 knot, $E(K) = 83.41$

between the ropelength or thickness and the proportion of the space in that component, as measured by the knot probability.

Graphs of probability versus ropelength, thickness, and energy show that this is not the case and suggest, rather, a possibly exponential relationship. An

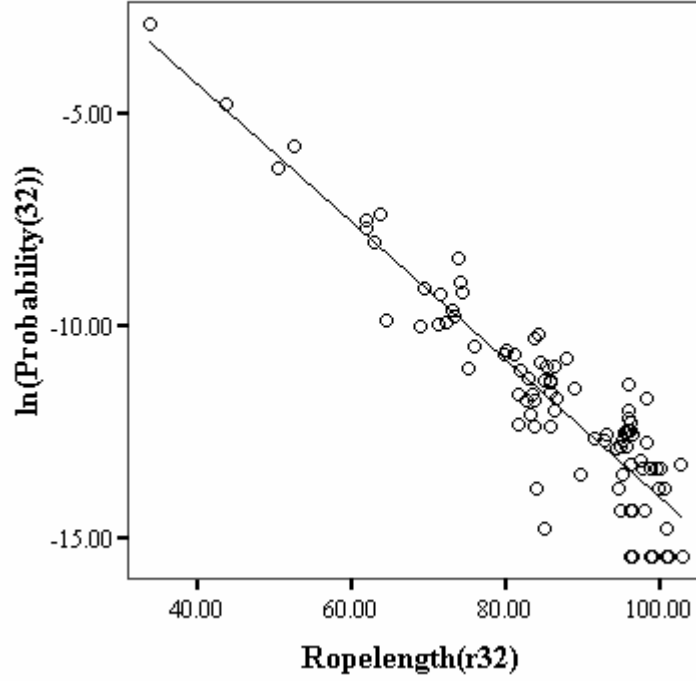


Fig. 20. $\ln(\text{probability}_{32})$ versus $\rho(K_{\rho_{32}})$

analysis of our data shows that,

$$Equ(32) : PR(K) = 9.03 e^{-0.16\rho(K_{\rho_{32}})}, R^2 = 0.85.$$

Thus, based on the data developed in this project, there appears to be no evidence that the probability of an equilateral knot type is simply related to the thickness, $\rho(K_{\rho_{32}})$, of the thickest representative of the knot type although the general trend is visible in Figure 20. Alternatively, this data might suggest that the component is not concentrated about the thickest representative but, rather, is somewhat dispersed in knot space.

Considering the possibility of a similar relationship between probability and energy gives a consistent structure,

$$Equ(32) : PR(K) = 0.091 e^{-0.05E_{MD}(K_{E_{32}})}, R^2 = 0.87.$$

One way in which to enclose a spatial knot is to construct a small box surrounding the knot and another is to take the convex hull of the knot. These data clearly suggest a linear relationship between the volume and surface areas of each of the encapsulating shapes. In each of the spaces $Equ(8)$, $Equ(16)$ and, $Equ(32)$ the data provides the following equations:

$$Equ(8) : BV(K_{\rho 8}) = -823.32 + 2.94 BSA(K_{\rho 8}), R^2 = 0.99,$$

$$Equ(16) : BV(K_{\rho 16}) = -806.12 + 2.90 BSA(K_{\rho 16}), R^2 = 0.98,$$

$$Equ(32) : BV(K_{\rho 32}) = -746.02 + 2.84 BSA(K_{\rho 32}), R^2 = 0.99.$$

where $BV(K) = BL(K) \cdot BW(K) \cdot BH(K)$ and $BSA(K) = 2(BL(K) \cdot BW(K) + BL(K) \cdot BH(K) + BW(K) \cdot BH(K))$.

If one changes the variables to L', W', H' by subtracting 5.91244, 5.883981, and 5.724601 from each of BL , BW , and BH in $Equ(8)$, $Equ(16)$, and $Equ(32)$, respectively, the following equations result:

$$Equ(8) : L'W'H' = 2.94 * 2(L'W' + L'H' + W'H'),$$

$$Equ(16) : L'W'H' = 2.90 * 2(L'W' + L'H' + W'H'),$$

$$Equ(32) : L'W'H' = 2.84 * 2(L'W' + L'H' + W'H').$$

By dividing, one has the following relationship between the dimensions of the box:

$$Equ(8) : 0.170068 = (1/L' + 1/W' + 1/H'),$$

$$Equ(16) : 0.172414 = (1/L' + 1/W' + 1/H'),$$

$$Equ(32) : 0.176056 = (1/L' + 1/W' + 1/H').$$

showing that the reciprocals of L' , W' and H' line in a plane.

This type of linear structure is not restricted to the case of an enclosing box. Let $HV(K)$ and $HSA(K)$ denote the volume and the surface area of the convex hull of K . In each of the spaces $Equ(8)$, $Equ(16)$, and $Equ(32)$ the data supports a linear relationship:

$$Equ(8) : HV(K_{\rho 8}) = -240.22 + 2.00 HSA(K_{\rho 8}), R^2 = 0.97,$$

$$Equ(16) : HV(K_{\rho 16}) = -239.03 + 2.07 HSA(K_{\rho 16}), R^2 = 0.96,$$

$$Equ(32) : HV(K_{\rho 32}) = -190.78 + 1.98 HSA(K_{\rho 32}), R^2 = 0.98.$$

Another manifestation of the special nature of the shape of the ropelength optimized knots is the relationship between $HVOL(K)$ and $\tau(K)$. In $Equ(32)$, we have

$$Equ(32) : HV(K_{\rho 32}) = -93.35 + 39614.10 \tau(K_{\rho 32}), R^2 = 0.98.$$

Alternatively,

$$Equ(32) : HV(K_{\rho 32}) = 209.63 + 36.09 \cdot \pi \tau(K_{\rho 32})^2, R^2 = 0.93,$$

providing a comparison between the volume of the convex hull and the volume of a torus neighborhood of the knot with radius equal to the thickness. This torus takes up approximately 1/36th of the volume suggesting a rather irregular position for the knot.

7 Connections to the Molecular Biology of DNA

Knotted molecular configurations occur in research studies designed to identify useful mechanisms describing the action of various classes of enzymes on DNA. Principal examples are the topoisomerases and enzymes mediating site-specific recombination. An understanding of the variation of the nature of knotting that arises under specific physical structural constraints is a useful tool in these studies. The coarsest grained structure is that of the polygonal knot for which there are no constraints on the length of edges, the angle between

adjacent edges, or other spatial constraints. Estimates based upon polygonal knots structure represent a limiting behavior. Equilateral knot space is a codimension n subspace of polygonal knot space. How does the structure of equilateral knot space compare with that of polygonal knot space? This is a complex question in as much as certain helpful aspects of the geometry and topology are inherited by the subspace. For example many local aspects of the structure of knots vary with the size of the perturbation in the same manner without respect to whether the knots are equilateral or merely polygonal. On the other hand, we know that the topological structure of the components of equilateral knot space is more complex than those of polygonal knot space [5]. This may imply that many elementary spatial properties may vary in a complicated fashion with the imposition of constraints on the angles or distinct families of subsets of equilateral knot space.

The central theme of the book, *Ideal Knots* [55], edited by A. Stasiak, V. Katritch, and L.H. Kauffman, is an exploration of whether there is a most “natural” representation of a knot type. While some elements of this discussion reflect a search for symmetry or visual simplicity, the underlying objective is the identification of conformations that arise most frequently, at least in some average manner, in the context of physical phenomena. Such “ideal” conformations are, it is proposed, those which provide optimal values for certain knot energies, for the thickness or the rope length, for the average crossing number, or for the ratio of knot volume divided by surface area. In the previous section we have discussed the interrelationships between the characteristics of such optimal conformations. One way by which the degree of success of these ideal conformations can be measured is through the comparison of the various spatial parameters and the electrophoretic separation of knots from the unknotted circle. This method is used by Stasiak, et al, in *Electrophoretic mobility of DNA knots* [2] derived from [56] and [57].

We wish to emphasize the disclaimer mentioned by Stasiak, et al. to the effect that the correlations observed between the real physical behaviour of DNA knots should not be construed as evidence that these represent the actual conformation. Only that these physical parameters appear to capture some characteristic of the “average” conformation that correlates to the physical behavior. In many cases, the development of a physical model that explains these observed relationships is the most important research objective in the mathematical domain.

Note that Stasiak et al. employ “mean inverse distances” and state that these are directly proportional to the average crossing numbers. “The mean of inverse distances in a molecule is an accepted measure of molecular compactness and is simply related to the sedimentation constant” [58].

In [59], they propose to demonstrate “that the expected sedimentation coeffi-

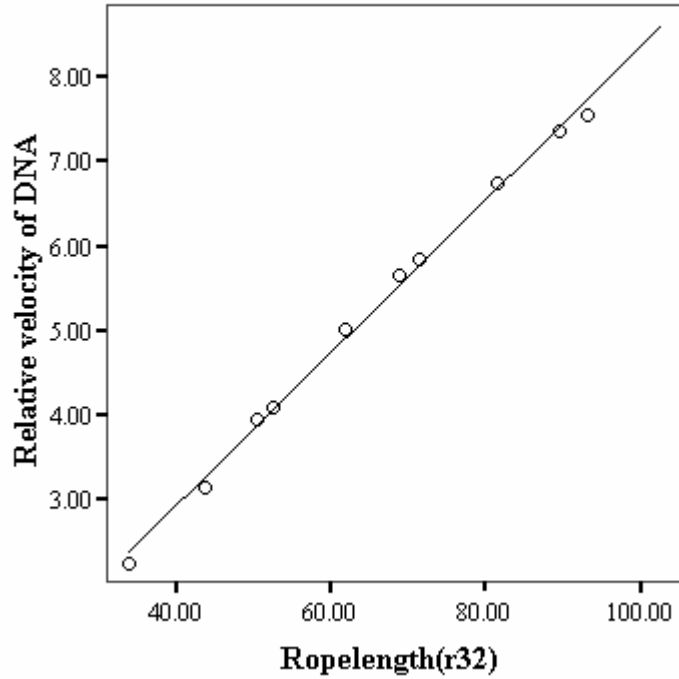


Fig. 21. Relative velocity of DNA versus $\rho(K_{\rho 32})$

cient of randomly fluctuating knotted or catenated DNA molecules in solution shows approximately linear correlation with the average crossing number of the corresponding knots or catenanes.” Later, “one of us (A.V.) developed recently a method to calculate the expected sedimentation coefficient of DNA molecules with a given topology [60].”

We see the same striking relationships between the ropelength, energy, average crossing number (optimized knots) and the gel mobility of the corresponding DNA knots. These relations are shown in Figures 21, 22, 23, and 24.

8 Conclusions, Conjectures, and Questions

One of the major objectives of this project has been the study of known relationships between physical knot parameters and the search for new relationships. From one point of view, we have developed evidence that implies the independence of many of these parameters. In other cases, for example ropelength and energy optimized knot configurations, the geometry of the knot is similar but not identical. Thus, similar but different properties of knots are connected. Finally, we have observed a few new relationships.

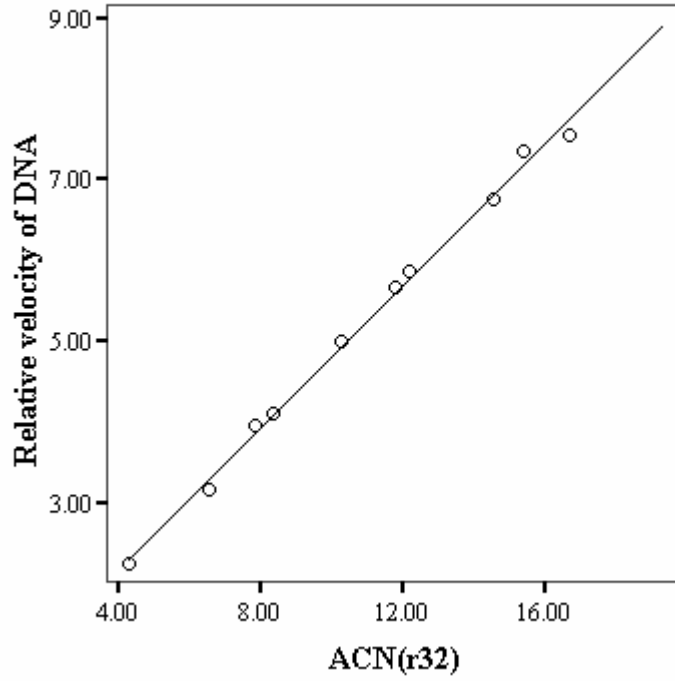


Fig. 22. Relative velocity of DNA versus $ACN(K_{\rho 32})$

One example of this is the apparent linear relationship between volume and surface area of optimal enclosing figures, boxes and convex hulls. While we are not able to prove this is the case, in general, we wish to propose the following conjecture:

Conjecture: There is a linear relationship between the volume and surface area of the ropelength optimized configurations of the equilateral knot types with the same number of edges;

and, propose the following question:

Question: What properties are implied by the existence of a linear relationship between the volume and surface area of a family of ropelength optimized equilateral knots?

In looking at the knot probability, we have observed the absence of a strong correlation between the size of the largest ball centered at the ropelength optimized knot and the probability. This suggests that the proportion of the volume, in a ball centered at this knot, of knots of the same geometric type falls off rapidly as the function of the radius. This is a measure of the degree of dispersal of the given knot type in knot space. As a consequence, we propose

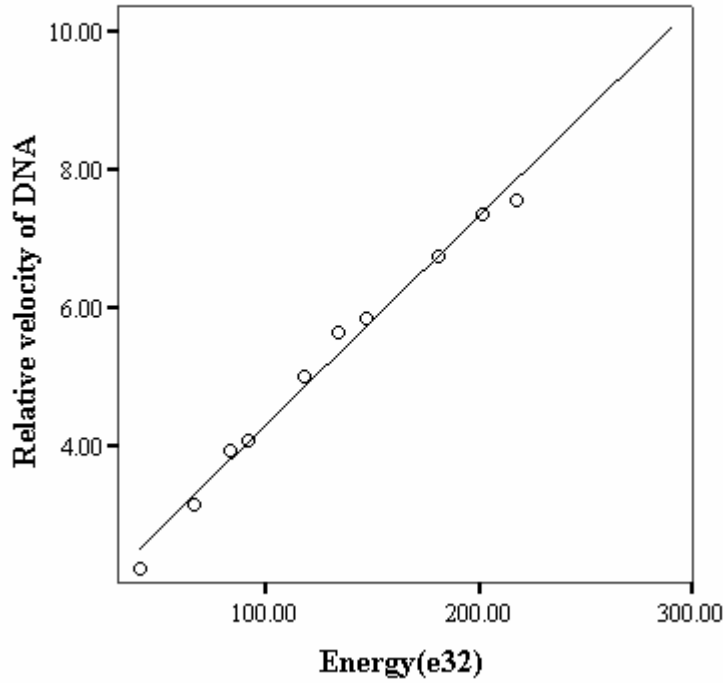


Fig. 23. Relative velocity of DNA versus $E_{MD}(K_{E32})$

the following question:

Question: What is the rate of dispersal of the knot types as a function of the radius of the ball centered at the minimal ropelength conformation (the conformation of maximal thickness)?

The geometric properties of the equilateral representatives (especially their optimized representatives) appear to undergo a phase transformation as a function of the number of edges. At one extreme, one has the minimal equilateral edge number model which is a very “tight” conformation. At the other extreme, one has models that closely approximate the ropelength optimized smooth knot of the same topological type. Our data provide preliminary evidence of the existence of this behavior and suggest some consequences in terms of the spatial nature of the equilateral model. Further research is required to demonstrate the existence of this transition and to capture and exploit potential connections between the behavior of the equilateral knots in the two regimes. One expected outcome is the ability to identify differences that strongly correlate with observed physical behavior such as gel mobility of DNA knots.

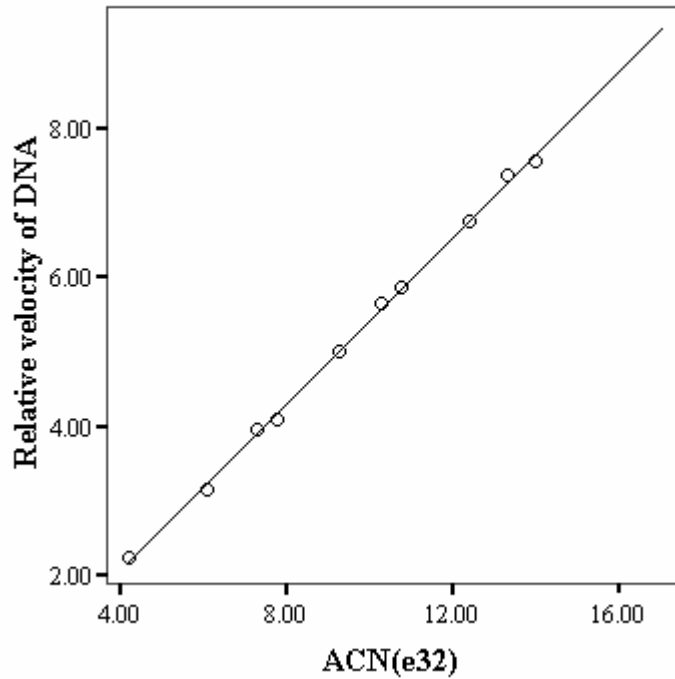


Fig. 24. Relative velocity of DNA versus $ACN(K_{E32})$

9 Acknowledgments

During Fall 1998 and Spring 1999, Kenneth Millett was on sabbatical visiting the Centre de Mathematiques et d' Informatique at the Universite de Provence, Marseille, France. He thanks the CMI and his colleagues there for their hospitality during the course of this research. Computational work was undertaken there and at the University of California, Santa Barbara. He thanks Stefan Boeriua and Joel Rising, at UCSB, for their extraordinary assistance in seeking new and creative ways in which to make this computational work possible. He wishes to thank his long time collaborator, Bruce Ewing, for his invaluable contributions to the HOMFLY knot polynomial program. Conversations with Jorge Alberto Calvo over the period of this research have had a significant influence on the direction and methods of this project.

Eric J. Rawdon's was supported in part by NSF grant #0074315 and Chatham College. He thanks the Chatham College Science Division for use of its SGI workstation used in many of the computations.

We thank our wives for their support and patience. We thank Rob Scharein for his help in installing KnotPlot, training us in KnotPlot, and writing the

scripts that created our initial conformations. We also thank Tom Hershberger for statistics and SPSS consultation.

References

- [1] V. Katritch, J. Bednar, D. Michoud, R. G. Scharein, J. Dubochet, A. Stasiak, Geometry and physics of knots, *Nature* 384 (6605) (1996) 142–145.
- [2] A. Stasiak, V. Katritch, J. Bednar, D. Michoud, J. Dubochet, Electrophoretic mobility of DNA knots, *Nature* 384 (1996) 122.
- [3] V. Katritch, W. K. Olson, P. Pieranski, J. Dubochet, A. Stasiak, Properties of ideal composite knots, *Nature* 388 (1997) 148–151.
- [4] A. Stasiak, J. Dubochet, V. Katritch, P. Pieranski, Ideal knots and their relation to the physics of real knots, in: *Ideal knots*, World Sci. Publishing, River Edge, NJ, 1998, pp. 1–19.
- [5] J. A. Calvo, Geometric knot theory: the classification of spatial polygons with a small number of edges, Ph.D. thesis, University of California, Santa Barbara (1998).
- [6] J. A. Calvo, The embedding space of hexagonal knots, preprint (1998).
- [7] J. A. Calvo, Geometric knot spaces and polygonal isotopy, preprint (1999).
- [8] K. C. Millett, Knotting of regular polygons in 3-space, in: *Random knotting and linking* (Vancouver, BC, 1993), World Sci. Publishing, River Edge, NJ, 1994, pp. 31–46.
- [9] K. C. Millett, D. W. Sumners (Eds.), *Random knotting and linking*, World Scientific Publishing Co. Inc., River Edge, NJ, 1994, papers from the AMS Special Session held in Vancouver, BC, August 15–19, 1993.
- [10] R. Randell, A molecular conformation space, in: R. Lacher (Ed.), *Studies in Physical and Theoretical Chemistry*, Vol. 54 of MATH/CHEM/COMP 1987, Elsevier Science, Amsterdam, 1988, pp. 125–140.
- [11] R. Randell, Conformation spaces of molecular rings, in: R. Lacher (Ed.), *Studies in Physical and Theoretical Chemistry*, Vol. 54 of MATH/CHEM/COMP 1987, Elsevier Science, Amsterdam, 1988, pp. 141–156.
- [12] H. Whitney, Elementary structure of real algebraic varieties, *Ann. of Math.* (2) 66 (1957) 545–556.
- [13] J. A. Calvo, K. C. Millett, Minimal edge piecewise linear knots, in: *Ideal knots*, World Sci. Publishing, River Edge, NJ, 1998, pp. 107–128.
- [14] K. C. Millett, Monte carlo explorations of polygonal knot spaces, preprint (1999).

- [15] Y. Diao, K. Ernst, E. Janse Van Rensburg, Energies of knots (March 1995).
- [16] Y. Diao, C. Ernst, E. J. Janse van Rensburg, In search of a good polygonal knot energy, *J. Knot Theory Ramifications* 6 (5) (1997) 633–657.
- [17] Y. Diao, C. Ernst, E. J. Janse van Rensburg, Knot energies by ropes, *J. Knot Theory Ramifications* 6 (6) (1997) 799–807.
- [18] Y. Diao, C. Ernst, E. J. Janse van Rensburg, Thicknesses of knots, *Math. Proc. Cambridge Philos. Soc.* 126 (2) (1999) 293–310.
- [19] M. H. Freedman, Z.-X. He, Z. Wang, Möbius energy of knots and unknots, *Ann. of Math.* (2) 139 (1) (1994) 1–50.
- [20] S. Fukuhara, Energy of a knot, in: *A fête of topology*, Academic Press, Boston, MA, 1988, pp. 443–451.
- [21] R. B. Kusner, J. M. Sullivan, Möbius energies for knots and links, surfaces and submanifolds, in: *Geometric topology* (Athens, GA, 1993), Amer. Math. Soc., Providence, RI, 1997, pp. 570–604.
- [22] R. B. Kusner, J. M. Sullivan, On distortion and thickness of knots, in: *Topology and geometry in polymer science* (Minneapolis, MN, 1996), Springer, New York, 1998, pp. 67–78.
- [23] O. Gonzalez, J. H. Maddocks, Global curvature, thickness, and the ideal shapes of knots, *Proc. Natl. Acad. Sci. USA* 96 (9) (1999) 4769–4773 (electronic).
- [24] J. O’Hara, Energy of a knot, *Topology* 30 (2) (1991) 241–247.
- [25] J. O’Hara, Family of energy functionals of knots, *Topology Appl.* 48 (2) (1992) 147–161.
- [26] J. O’Hara, Energy functionals of knots, in: *Topology Hawaii* (Honolulu, HI, 1990), World Sci. Publishing, River Edge, NJ, 1992, pp. 201–214.
- [27] J. O’Hara, Energy functionals of knots. II, *Topology Appl.* 56 (1) (1994) 45–61.
- [28] J. K. Simon, Energy functions for polygonal knots, *J. Knot Theory Ramifications* 3 (3) (1994) 299–320, random knotting and linking (Vancouver, BC, 1993).
- [29] E. Rawdon, The thickness of polygonal knots, Ph.D. thesis, University of Iowa (1997).
- [30] E. J. Rawdon, Approximating the thickness of a knot, in: *Ideal knots*, World Sci. Publishing, River Edge, NJ, 1998, pp. 143–150.
- [31] E. J. Rawdon, Approximating smooth thickness, *J. Knot Theory Ramifications* 9 (1) (2000) 113–145.
- [32] R. A. Litherland, J. Simon, O. Durumeric, E. Rawdon, Thickness of knots, *Topology Appl.* 91 (3) (1999) 233–244.

- [33] E. Rawdon, J. Simon, Polygonal approximation and energy of smooth knots, preprint (2000).
- [34] J. W. Milnor, On the total curvature of knots, *Ann. of Math.* (2) 52 (1950) 248–257.
- [35] W. Fenchel, Über Krümmung und Windung geschlossener Raumkurven, *Annals of Mathematics* 101 (1929) 238–252.
- [36] E. Pannwitz, Eine freie Abbildung der n -dimensionalen Sphäre in die Ebene, *Math. Nachr.* 7 (1952) 183–185.
- [37] H. R. Morton, D. M. Q. Mond, Closed curves with no quadriseccants, *Topology* 21 (3) (1982) 235–243.
- [38] D. Mond, Looking at bent wires— \mathcal{A}_e -codimension and the vanishing topology of parametrized curve singularities, *Math. Proc. Cambridge Philos. Soc.* 117 (2) (1995) 213–222.
- [39] G. Kuperberg, Quadriseccants of knots and links, *Journal of Knot Theory and Its Ramifications* 3 (1994) 41–50.
- [40] N. Metropolis, A. Rosenbluth, M. Rosenbluth, A. Teller, E. Teller, Equation of state calculations by fast computing machines, *The Journal of Chemical Physics* 21 (1953) 1087–1092.
- [41] P. Freyd, D. Yetter, J. Hoste, W. B. R. Lickorish, K. Millett, A. Ocneanu, A new polynomial invariant of knots and links, *Bull. Amer. Math. Soc. (N.S.)* 12 (2) (1985) 239–246.
- [42] W. B. R. Lickorish, K. C. Millett, A polynomial invariant of oriented links, *Topology* 26 (1) (1987) 107–141.
- [43] J. Hoste, M. Thistlethwaite, J. Weeks, The first 1,701,936 knots, *Math. Intelligencer* 20 (4) (1998) 33–48.
- [44] R. Scharein, Knotplot, <http://www.cs.ubc.ca/spider/scharein>, program for drawing, visualizing, manipulating, and energy minimizing knots.
- [45] E. Rawdon, Toros, <http://monkey.chatham.edu/~rawdon>, program for visualizing, manipulating, and thickness maximizing knots.
- [46] Y.-Q. Wu, Ming, <http://www.math.uiowa.edu/~wu>, program for visualizing, manipulating, and energy minimizing polygonal knots.
- [47] J. Simon, J. Tockle, Critical values of energy functions (1999).
- [48] T. Banchoff, Self linking numbers of space polygons, *Indiana Univ. Math. J.* 25 (12) (1976) 1171–1188.
- [49] B. Ewing, K. C. Millett, Computational algorithms and the complexity of link polynomials, in: *Progress in knot theory and related topics*, Hermann, Paris, 1997, pp. 51–68.

- [50] F. Jaeger, D. L. Vertigan, D. J. A. Welsh, On the computational complexity of the Jones and Tutte polynomials, *Math. Proc. Cambridge Philos. Soc.* 108 (1) (1990) 35–53.
- [51] J. Hoste, personal communication (2000).
- [52] G. Buck, E. Rawdon, J. Simon, Conformal energy of thick knots, submitted (October 1999).
- [53] G. Buck, Four-thirds power law for knots and links, *Nature* 392 (1998) 238–239, scientific Correspondence.
- [54] P. Pierański, In search of ideal knots, in: *Ideal knots*, World Sci. Publishing, River Edge, NJ, 1998, pp. 20–41.
- [55] A. Stasiak, V. Katritch, L. H. Kauffman (Eds.), *Ideal knots*, World Scientific Publishing Co. Inc., River Edge, NJ, 1998.
- [56] N. J. Crisona, R. Kanaar, T. N. Gonzalez, E. L. Zecheidrich, A. Klippel, N. R. Cozzarelli, Processive recombination by wild-type Gin and an enhancer-independent mutant. Insight into the mechanisms of recombination selectivity and strand exchange, *J. Mol. Biol.* 243 (3) (1994) 437–457.
- [57] R. Kanaar, A. Klippel, E. Shekhtman, J. M. Dungan, R. Kahmann, N. R. Cozzarelli, Processive recombinations by the phage Mu Gin system: implications for the mechanisms of DNA strand exchange, DNA site alignment and enhancer action, *Cell* 62 (2) (1990) 353–366.
- [58] M. Le Bret, Monte Carlo computation of the supercoiling energy, the sedimentation constant, and the radius of gyration of unknotted and knotted circular DNA, *Biopolymers* 19 (3) (1980) 619–637.
- [59] A. V. Vologodskii, N. J. Crisona, B. Laurie, P. Pieranski, V. Katritch, J. Dubochet, A. Stasiak, Sedimentation and electrophoretic migration of DNA knots and catenanes, *J. Mol. Biol.* 278 (1) (1998) 1–3.
- [60] V. V. Rybenkov, A. V. Vologoskii, N. R. Cozarelli, The effect of ionic conditions on the conformations of supercoiled DNA. I. Sedimentation analysis, *J. Mol. Biol.* 267 (2) (1997) 299–311.